IEEE Access
Multidisciplinary ⋮ Rapid Review ⋮ Open Access Journal

Received 31 December 2023, accepted 15 January 2024, date of publication 23 January 2024, date of current version 1 February 2024.

Digital Object Identifier 10.1109/ACCESS.2024.3357741

RESEARCH ARTICLE

Hybrid Transient Search Algorithm With Levy Flight for Optimal PI Controllers of Islanded Microgrids

AHMED M. HUSSIEN[1], HANY M. HASANIEN[2,1], (Senior Member, IEEE), MOHAMMED H. QAIS[3], (Member, IEEE), AND SAAD ALGHUWAINEM[4], (Senior Member, IEEE)

[1]Electrical Engineering Department, Faculty of Engineering and Technology, Future University in Egypt, Cairo 11835, Egypt
[2]Electrical Power and Machines Department, Faculty of Engineering, Ain Shams University, Cairo 11517, Egypt
[3]Centre for Advances in Reliability and Safety, Hong Kong, China
[4]Electrical Engineering Department, College of Engineering, King Saud University, Riyadh 11421, Saudi Arabia

Corresponding author: Hany M. Hasanien (hanyhasanien@ieee.org)

This work was supported by the Deputyship for Research and Innovation, Ministry of Education, Saudi Arabia, under Grant IFKSUOR3-328-2.

ABSTRACT This study combines the metaheuristic algorithm Transient Search Optimization (TSO) with the Levy flight distribution to find the optimal proportional-integral (PI) controllers for robust operation of islanded microgrids. The first step is to use the response surface methodology (RSM) to empirically express the multi-objective function. This function includes the transient variations of the terminal voltages of the microgrids. To demonstrate the efficacy of the hybrid Levyflight and TSO (LTSO), a benchmark microgrid system undergoes rigorous testing under different operational scenarios: i) transitioning the system into autonomous mode by disconnecting from the main grid; ii) adapting to varying load conditions while isolated; and iii) responding to a 3-phase fault while operating in islanded mode. Numerous simulations are run to verify the suggested methodology, employing conventional data extracted from the PSCAD/EMTDC software. The study's findings are further reinforced through a comparative analysis with established optimization techniques such as the least mean and the square root of exponential approaches, the enhanced block-sparse adaptive Bayesian algorithm, the adaptive-width generalized correntropy diffusion algorithm, the sunflower optimization algorithm, the Coot bird metaheuristic optimizer, and particle swarm optimization. The results collectively underscore the superiority of the LTSO algorithm in enhancing the transient response of the terminal voltages of islanded microgrids, thereby offering a promising avenue for optimizing the control and stability of such systems.

INDEX TERMS Coot bird metaheuristic optimizer, distributed generators, renewable energy, microgrid, sunflower optimization algorithm.

I. INTRODUCTION

A. LITERATURE SURVEY

The modern energy environment is transforming remarkably, characterized by an ever-growing demand for electric power and a rising concern for environmental sustainability. This shift has encouraged the widespread adoption of distributed energy resources (DERs), including technologies such as fuel cells, photovoltaic (PV) systems, micro-turbines, and wind farms [1], [2], [3], [4]. Regarding distributed generation, these technologies are typically connected to the electric grid through voltage source inverters (VSIs) [5], marking a departure from the conventional synchronous generators (SGs).

This transition from SGs to DERs introduced a significant change in the energy sector, given that VSIs and DERs own distinct physical characteristics and operational

The associate editor coordinating the review of this manuscript and approving it for publication was Qiang Li.

requirements. Unlike SGs, which benefit from their substantial spinning mass and high inertia, contributing to grid stability by maintaining grid frequency, distributed generators (DGs) face unique challenges due to their lack of rotational mass and inertia. This absence of inertia necessitates innovative approaches to address grid stability concerns, including integrating energy storage systems and developing suitable regulatory frameworks. The microgrid (MG) concept has emerged as a promising solution to address these challenges.

The concept of an MG stands at the core of the evolving energy environment, representing a developed and controlled structure composed of multiple DGs, various loads, and integrated energy storage devices, all interconnected within a local network. The MGs can operate in two distinctive modes: autonomous and grid-connected, addressing diverse energy challenges [6].

One of the distinguishing features of microgrids is their strategic placement near energy demand centers. This nearness minimizes transmission losses and establishes a robust structure for providing a consistent and reliable power supply to the surrounding area. A significant characteristic of Microgrids is their ability to enhance the collaborative integration of numerous Renewable Energy Sources (RESs) in a distributed manner, thus significantly improving the energy supply's reliability.

In the grid-connected mode, the operational parameters of Microgrids, including voltage and frequency, are typically governed by the centralized electrical grid. However, the scenario changes dramatically when an MG transitions into the islanded mode, operating independently from the primary grid. In this autonomous mode, the VSIs become the hub responsible for sustaining these crucial parameters [7], [8], [9]. The transition from grid-connected to islanded mode presents new challenges and complexities in controlling and managing VSI interfaces [10], [11]. This shift underscores the necessity for advanced control strategies (CS) and technologies that can effectively guide MG operations in a self-reliant manner.

In the dynamic world of DG and MG management, the efficacy of CS plays an essential role in ensuring operational reliability and stability. Advanced CSs have become crucial, particularly in the off-grid mode, where the reliability and precision of operation are dominant. To address the complicated challenges of control in this context, a range of CSs falls into three primary categories: droop-based control (DCL), centralized control (CCL), and multivariable and servomechanism (MVASM) techniques.

Inspired by the characteristics of SGs, Droop-based control empowers peer-to-peer control, granting the notable ability to independently manage the power output of individual DG units without necessitating extensive coordination or interaction among these units. A wireless CS focusing on P-Q droop organization emerges as a promising solution, offering decentralized management of distributed units with minimal interaction among them [12]. This approach stands out for its robustness and consistency, surpassing other power-sharing and MG frequency regulation methods [13]. However, the efficacy of droop control in low-voltage MGs with resistor line impedance is notably affected by power couplings [14], presenting a challenge that necessitates innovative solutions such as the virtual vector transformation technique [15], though with potential stability impact.

Centralized CS, on the other hand, offers precise and coordinated control, but it demands high-bandwidth interconnections. The reliance on these interconnections introduces a vulnerability, as any breakdown in communication links can lead to microgrid failure. Recent advancements in the field have explored autonomous communication-based centralized control for DC MGs, enhancing their resilience and adaptability [16]. To conclude, it is worth noting that while a novel approach has been proposed for the development of MVASM designed to handle multi-input/output stable systems [17], it is essential to acknowledge that the inherent complexity of this approach can present significant challenges. While holding promise for advanced control in complex systems, this complexity may require careful consideration and refinement to make it a practical and effective solution in real-world applications.

In dealing with nonlinear problems of the MG context, the proportional-integral controller (PIC) emerges as a frequently employed solution due to its inherent stability margin. However, the PIC faces challenges related to parameter fluctuations and network nonlinearity, posing a significant obstacle in determining appropriate PIC settings within these complex and dynamic systems.

B. RESEARCH GAP AND MOTIVATION

In recent years, the booming importance of MG systems in the ever-evolving system has prompted extensive research efforts to design optimal controllers to ensure their successful and efficient operation. Among the CSs, PICs have emerged as a fundamental tool in managing MGs, particularly when maintaining the voltage of Voltage Source Converters within a d-q axis [18]. One key challenge with PICs arises when assuming linearity in the system, as these controllers are often tuned using conventional methods like the Zigler-Nicholas method [19]. However, this linearity assumption doesn't hold in all practical scenarios, leading to saturation outcomes and a consequential reduction in control stability margin, often coupled with significant phase lag. Moreover, the dynamic nature of MGs, with parameters and operating conditions subject to frequent changes [20], A distributed PIC to control the powers of an electric system is shown in [21]. Raises an additional obstacle for controllers. Researchers have invented many advanced optimization techniques to address these complications and optimize the control of MGs. Such as Enhanced Transient Search Optimization [22], the Coot bird metaheuristic optimizer (COOT) [19], the Enhanced Bald Eagle Search Algorithm [23], genetic algorithms [24], modified virtual rotor-based derivative technique supported with Jaya optimizer based on balloon effect [25], the Adaptive-Width

Generalized Correntropy Diffusion Algorithm (AWGC-DA) [26], the Sunflower (SFO) algorithm [27], Enhanced Block-Sparse Adaptive Bayesian algorithm (EBS-ABA) [28], the Cuttlefish optimization algorithm [29], the ant colony algorithm [30], Circle Search Algorithm [31], the particle swarm optimization (PSO) [32], [33], and The least mean (LM) and the square root of exponential (SRE) [6]. These optimization methods aim to enhance decentralized controllers in MG systems, fine-tune parameters, and improve performance. Nevertheless, it's crucial to acknowledge that each method has advantages and disadvantages [34]. Despite the ongoing research efforts, no universal framework for MG control has yet been established.

C. CONTRIBUTION AND PAPER BODY

This research presents an innovative methodology for optimizing CSs within islanded MGs by harnessing the capabilities of the LTSO technique. This study's primary focus involves determining optimal gains for PICs by applying LTSO within a multi-objective optimization framework. To enhance the robustness and effectiveness of the approach, the Response Surface Methodology (RSM) is integrated into the procedure to achieve a balanced solution across various conflicting objectives. The study's findings are further reinforced through a comparative analysis with established optimization techniques such as LMSRE, EBS-ABA, AWGC-DA, SFO, COOT, and PSO.

This paper adds to filling the previously indicated deficiencies:

1) Evolving an innovative methodology based on LTSO to determine optimal gains for PICs to enhance the MG system's reliability,
2) Demonstrate the efficacy of this innovative LTSO-based methodology by exposure to a benchmark MG system and rigorous testing under different operational scenarios: i) transitioning the system into autonomous mode by disconnecting from the primary grid, ii) adapting to varying load conditions while isolated, and iii) responding to a 3-phase fault while operating in islanded mode,
3) Enhancing the solidity of the presented optimizer through a comparative analysis with established optimization techniques such as LMSRE, EBS-ABA, AWGC-DA, SFO, COOT, and PSO.

This article is structured into distinct sectors to provide a coherent and comprehensive exploration of the subject matter. The following is the organization of the paper:

Sector I: Introduction, Sector II: Microgrid Demonstration, Sector III: Control Plan, Sector IV: Design Procedures, Sector V: Optimization Strategies and Modeling, Sector VI: Simulation Results and Discussion, and Sector VII: Conclusion.

II. MG DEMONSTRATING

Figure 1 provides a single-line diagram illustrating the configuration of an MG. This diagram is instrumental in visualizing the key components and connections within the MG system. The MG comprises three DG units, which are represented in the diagram. These DGs serve as local power sources within the MG. Each DG is interconnected by transmission lines ($R_{TL1} = 0.7\ \Omega$, $R_{TL2} = 1.5\ \Omega$, $L_{TL1} = 0.5$ mH, and $L_{TL2} = 0.9$ mH). These lines enable the exchange of electrical power between the DG units, contributing to the stability and reliability of the MG. The MG is connected to the utility grid (V = 13.8 KV, $R_g = 0.2\ \Omega$, $L_g = 0.3$ mH) through a Point of Common Coupling (PCC). This connection allows for the import and export of electrical power between the MG and the utility grid. It is a vital interface for grid-connected operations. Each DG includes a DC supply system (VDC = 600 V) linked to a Pulse Width Modulation (PWM) inverter. The PWM system typically operates with two levels, facilitating precise control over the power supplied by the DG. The AC supplied from each PWM inverter is connected to a Δ-Y transformer (0.6/13.8 KV). A filter Z_f($R_f = 1.5$ mΩ, $X_f = 0.5$ mH) is inserted in the connection path between the PWM inverter and the transformer to maintain power quality and avoid issues related to voltage and current harmonics. After the transformer, an R($R_{Ll2,}$ R_{L21}, R_{L31}, R_{Ll1}, R_{L22}, and R_{L33} = 150, 150, 150, 9, 5, and 20 Ω)L(L_1, L_2, and L_3 = 0.6, 0.4, 1.5 H)C(C_1, C_2, and C_3 = 50, 42, and 33 μF) is integrated into the system. This load represents the local electrical demand within the MG.

This study focuses on improving the off-grid operation of the MG by implementing a cascaded control method. This control method is detailed and discussed in depth in the next section.

III. CONTROL PLAN

The control system for the MG in this study is designed with a cascading control technique, comprising two layers of control, each with specific responsibilities and functions depending on the operational mode of the MG, which is presented in Figure 2.

In the grid-connected mode, the outer control layer manages the complex powers of the MG, maintaining the desired power output. Concurrently, the inner control layer focuses on adjusting the direct and quadrature (d-q) current components ($I_{conv.\_d}$, $I_{conv.\_q}$) to control the voltages at the PCC. This inner control layer plays a critical role in regulating voltage levels at the PCC while operating in grid-tied mode.

In the islanded mode, the control system adapts. In this mode, the outer layer controls the d-q voltages (V_q, V_d). The inner control layer continues to manage the d-q currents. A transformation process is used to convert the d-q reference voltages ($V_{conv.\_d}*$, $V_{conv.\_q}*$) into reference voltages in the ABC coordinate system ($V_{conv.\_a}*$, $V_{conv.\_b}*$, $V_{conv.\_c}*$). The control system employs four PICs for generating the d-q reference voltages ($V_{conv.\_d}*$ and $V_{conv.\_q}*$).

To implement the control actions, the inverter uses a comparator. The comparator compares a triangle waveform (1980 HZ) [28] to the reference voltages ($V_{conv.\_d}*$ and $V_{conv.\_q}*$). This comparison drives the inverter's switching actions, controlling the output to maintain the desired voltage and power

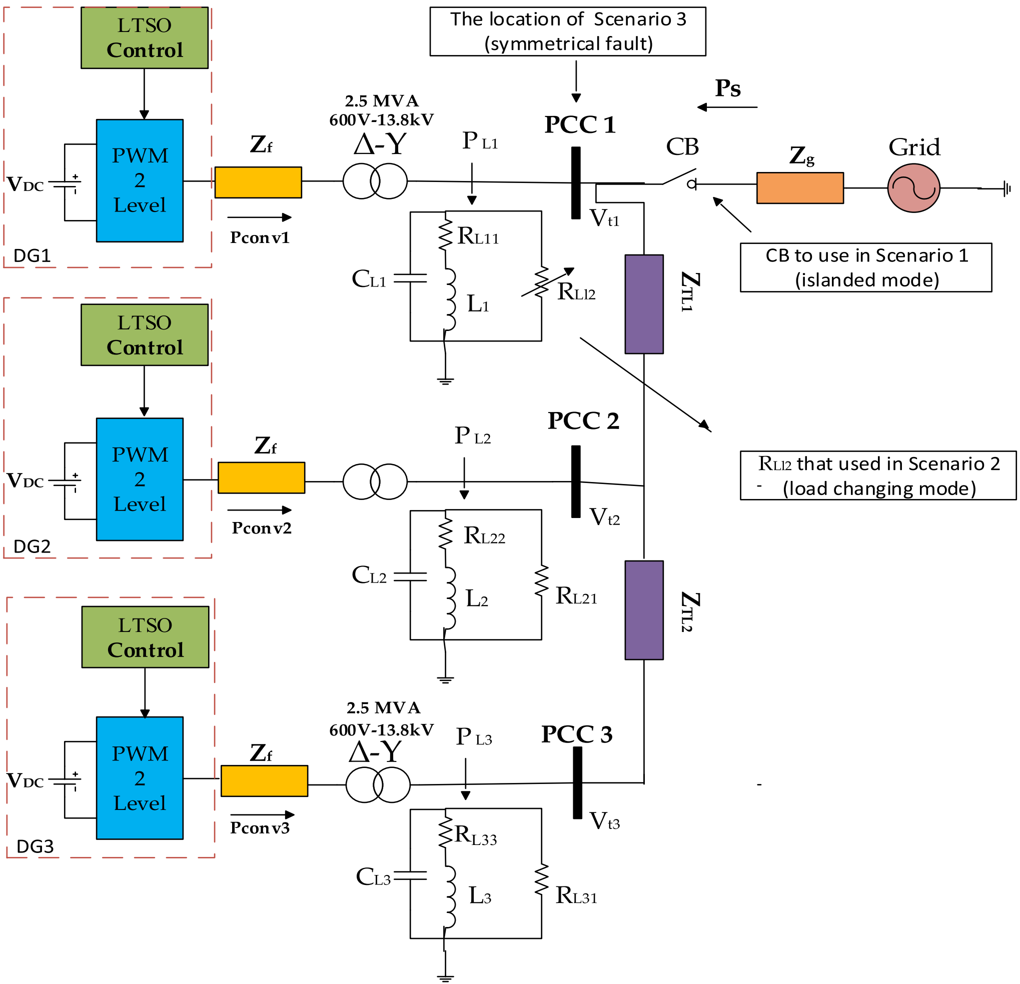

FIGURE 1. The utilized MG.

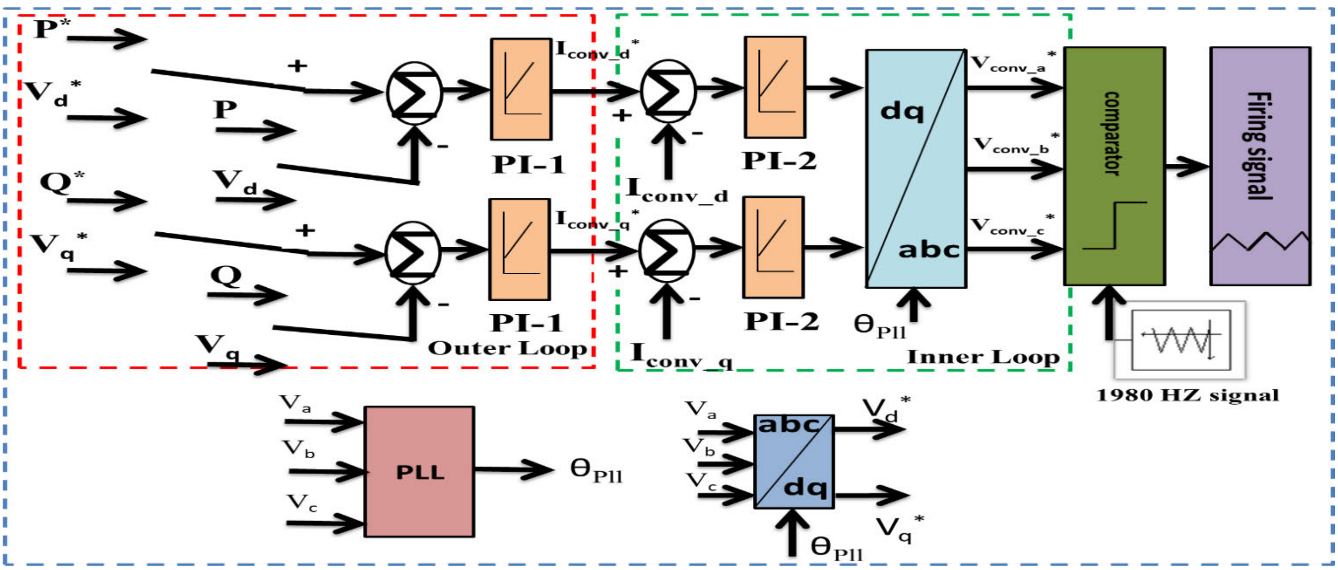

FIGURE 2. The cascaded control scheme for the MG.

profiles. The parameters of the PICs are determined and optimized using the LTSO technique. This ensures the control system is finely tuned to achieve the desired performance.

The control system's structure and operation are adaptable to the MG's mode of operation, effectively managing both power and voltage levels to ensure the MG operates with stability and precision. Stability ensures the system operates without oscillations or disruptions, while precision implies accurate control of power and voltage levels. The following section of the study will provide more in-depth details about the PICs.

IV. DESIGN PROCEDURES

A. SELECTION OF VARIABLES

The PICs employed in this article are configured within the MG's three DGs. Each DG is equipped with two PICs, resulting in a total of six PICs, which are designated as follows: For DG1: $PI_{1.1}$, and $PI_{1.2}$, For DG2: $PI_{2.1}$, and $PI_{2.2}$, and For DG3: $PI_{3.1}$, and $PI_{3.2}$.

These PICs are responsible for controlling various aspects of the DGs' operation to ensure the stability and desired performance of the MG.

The PICs used in this research have two crucial parameters: Proportional Gain (KP):

- For $PI_{1.1}$ in DG_1, represented as R_1.
- For $PI_{1.2}$ in DG_1, represented as R_3.
- For $PI_{2.1}$ in DG_2, represented as R_5.
- For $PI_{2.2}$ in DG_2, represented as R_7.
- For $PI_{3.1}$ in DG_3, represented as R_9.
- For $PI_{3.2}$ in DG_3, represented as R_{11}.

Integral Time Constant (TI):

- For $PI_{1.1}$ in DG_1, represented as R_2.
- For $PI_{1.2}$ in DG_1, represented as R_4.
- For $PI_{2.1}$ in DG_2, represented as R_6.
- For $PI_{2.2}$ in DG_2, represented as R_8.
- For $PI_{3.1}$ in DG_3, represented as R_{10}.
- For $PI_{3.2}$ in DG_3, represented as R_{12}.

Additionally, the control system uses three levels to categorize the variables associated with the controllers, as stated in Table 1. These levels help define safe operating boundaries and reference points for the PICs, ensuring they operate within acceptable and safe limits. The combination of the specific PICs, associated KP and TI values, and the defined control levels form a structured control system for the MG.

B. The RSM AND MINITAB SOFTWARE

A simulation of the MG system is carried out using PSCAD software. The RSM uses the information extracted from these simulations to create its inputs. The RSM is a robust mathematical procedure [35] employed in this study to empirically construct models that expose the intricate relationships between control strategies and the dynamic behavior of the MG. The essential input data for RSM consists of critical parameters that evaluate the MG's performance. These parameters include the steady-state error (E_{sse}), the maximum percentage under/overshoots (MPUT/MPOT), and the settling time (T_{stl}), which are incorporated as a critical input for RSM and are stated in the appendixes Tables 6- 8. To assemble and analyze these empirical models, data from PSCAD simulations is employed, describing the MG's diverse behaviors under different operational conditions. MINITAB is the software used for the construction of RSM models.

TABLE 1. Boundary levels.

Gains Levels	(−1)	(0)	(1)
R_1	1	4.5	8
R_2	0.0001	0.04505	0.09
R_3	1.3	2.4	3.5
R_4	0.02	1.11	2.2
R_5	0.8	4.15	7.5
R_6	0.00015	0.047575	0.095
R_7	1	2.1	3.2
R_8	0.01	1.155	2.3
R_9	0.5	3.75	7
R_{10}	0.00012	0.04656	0.093
R_{11}	0.9	1.95	3
R_{12}	0.009	1.2545	2.5

The multi-objective function in this study aims to minimize specific performance metrics for the MG system under consideration. These performance metrics include B_1 (MPOT), B_2 (MPUT), B_3 (T_{stl}), and B_4 (E_{sse}). Equation (1) defines the multi-objective function as a second-order polynomial RSM template.

$$B_i = C_1 + C_2R_1 + C_3R_2 + C_4R_3 + C_5R_4 + C_6R_1^2 + C_7R_2^2 + C_8R_3^2 + C_9R_4^2 + C_{10}R_1R_2 + C_{11}R_1R_3 + C_{12}R_1R_4 + C_{13}R_2R_3 + C_{14}R_2R_4 + C_{15}R_3R_4 \quad (1)$$

where $i = 1, 2, 3, 4$, and $C_1, C_2 \ldots, C_{15}$ are the figured RSM coefficients for the scenarios stated in the appendixes Tables 9-11.

V. OPTIMIZATION STAGE

Eq. (1) employs the weighting approach [36] as an input to the LTSO, COOT, SFO, and PSO approaches to get the most effective PI parameters while minimizing transients. The number of iterations for LTSO, COOT, SFO, and PSO is 500, and the search agents are 20. Table 2 shows the weights used in this study. The results of the LMSRE, EBS-ABA, AWGC-DA, SFO, COOT, and PSO are extracted from [26] and compared with the results of the proposed technique explained in the next section.

A. TSO

The TSO, informed in 2020 by Qais M [37], is a novel and promising meta-heuristic optimization approach rapidly gaining attention in renewable energy. It has been applied to test various optimization challenges, demonstrating its versatility and effectiveness. The TSO technique's origin can be traced to the study of transient performance in electrical circuits containing energy storage elements, such as capacitors and inductors.

TABLE 2. The weights.

Weights (W)	DG #		
W_1		B_1	0.2
W_2	DG_1	B_2	0.2
W_3		B_3	0.075
W_4		B_4	0.03
W_5		B_5	0.125
W_6	DG_2	B_6	0.125
W_7		B_7	0.04
W_8		B_8	0.02
W_9		B_9	0.075
W_{10}	DG_3	B_{10}	0.075
W_{11}		B_{11}	0.025
W_{12}		B_{12}	0.01

In electrical circuits, changes in the parameters, like inductor currents and capacitor voltages, do not occur instantaneously after a switching event due to the presence of these energy storage elements. This delayed response is referred to as the transient response of the circuits. To utilize the potential of the TSO technique, the [37]authors drew inspiration from its foundations in modeling and optimizing the transient behavior of electrical systems. This method has shown promise in solving optimization problems in the renewable energy domain, including estimating the electrical parameters of photovoltaic modules [38] and proton exchange membrane fuel cells [39]. Therefore, it serves as a valuable tool for enhancing the performance and efficiency of the MG system in this research.

The order of the circuits affects their transient responsiveness. The transient response of first-order circuits may be expressed numerically, as illustrated in equation (2). equation (3) shows the answer to equation (2):

$$\frac{d}{dt}z(t) + \frac{z(t)}{\tau} = K \tag{2}$$

$$z(t) = z(\infty) + (z(0) - z(\infty))e^{\frac{-t}{\tau}} \tag{3}$$

Likewise, under transients, second-order circuits may be formally described by the second-order differential equation illustrated below:

$$\frac{d^2}{dt^2}z(t) + 2\alpha\frac{d}{dt}z(t) + \omega_0^2 z(t) = f(t) \tag{4}$$

Equation (5) shows the answer to equation (4):

$$z(t) = e^{-\alpha t}\left(N_1 cos\left(2\pi f_d t\right) + N_2 sin\left(2\pi f_d t\right)\right) + z(\infty) \tag{5}$$

where z(t) is the dynamic measurement of the voltage over the capacitance of the circuit or the current in the inductor of the circuit, τ is a time constant. The damping coefficient is denoted by α. The resonant and damped frequencies are denoted by ω_0 and f_d, respectively. N_1 and N_2 are constants. The TSO's search agents are updated, as illustrated in (6). This equation is the mathematical formulation of the TSO technique's exploration and extraction phases.

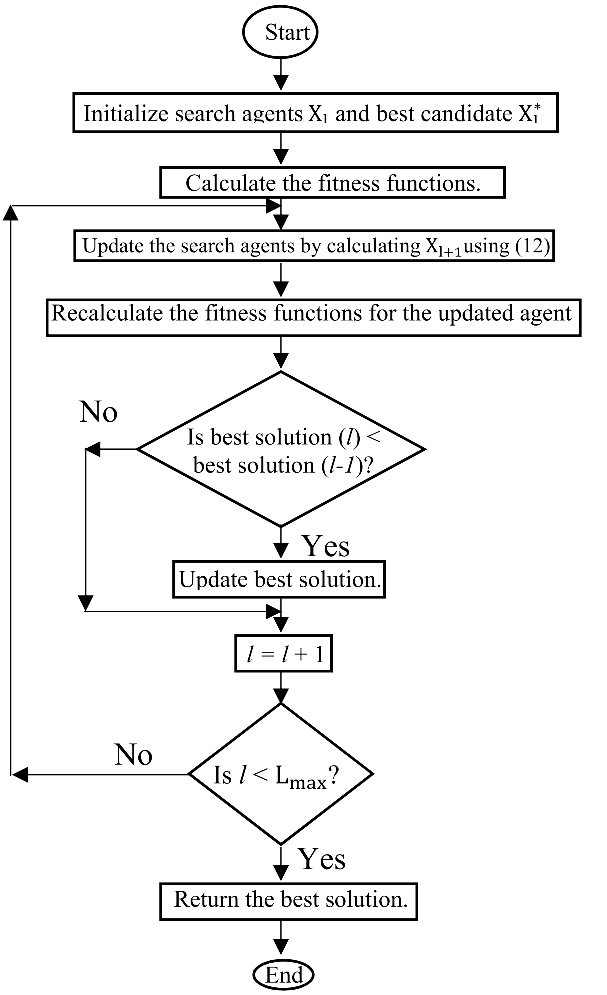

FIGURE 3. Flowchart of LTSO algorithm.

$$X_{l+1} = \begin{cases} X_l^* + \left(X_l - D_1.X_l^*\right)e^{-T} & r_1 < 0.5 \\ X_l^* + e^{-T}\left[cos\left(2\pi T\right) + sin\left(2\pi T\right)\right] \\ \left|X_l - D_1.X_l^*\right| & r_1 \geq 0.5 \end{cases} \tag{6}$$

$$T = 2 \times a \times r_2 - a \tag{7}$$

$$C_1 = k \times a \times r_3 + 1 \tag{8}$$

$$a = 2 - 2(^{l}/_{L_{max}}) \tag{9}$$

All randomized numbers are t, D_1, r1, r2, and r3. X_l reflects the population's location. The best position is represented by X_l^*. The letter l represents the number of iterations. k is a constant. The 'T' factor balances the exploration and extraction phases. 'T' has a range of [−2, 2]. When 'T' is positive, the extraction process is dominating. Alternatively, a negative value for 'T' indicates that exploration dominates.

B. HYBRID TSO WITH LEVY FLIGHT

Adjustments to the method by which the search agents are updated are implemented to improve the performance of the suggested TSO methodology. The initial search agents have been modified to include the Levy and Weibull functions.

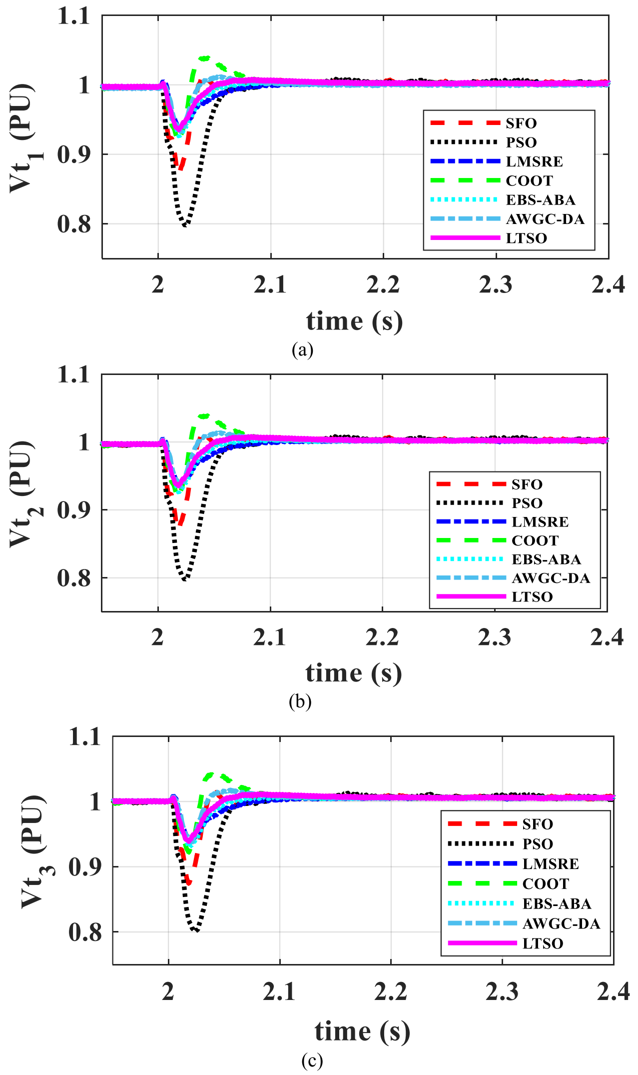

FIGURE 4. The LTSO, LMSRE, EBS-ABA, AWGC-DA, SFO, COOT, and PSO voltages for Scenario 1. (a-c) are for DG_1 to DG_3.

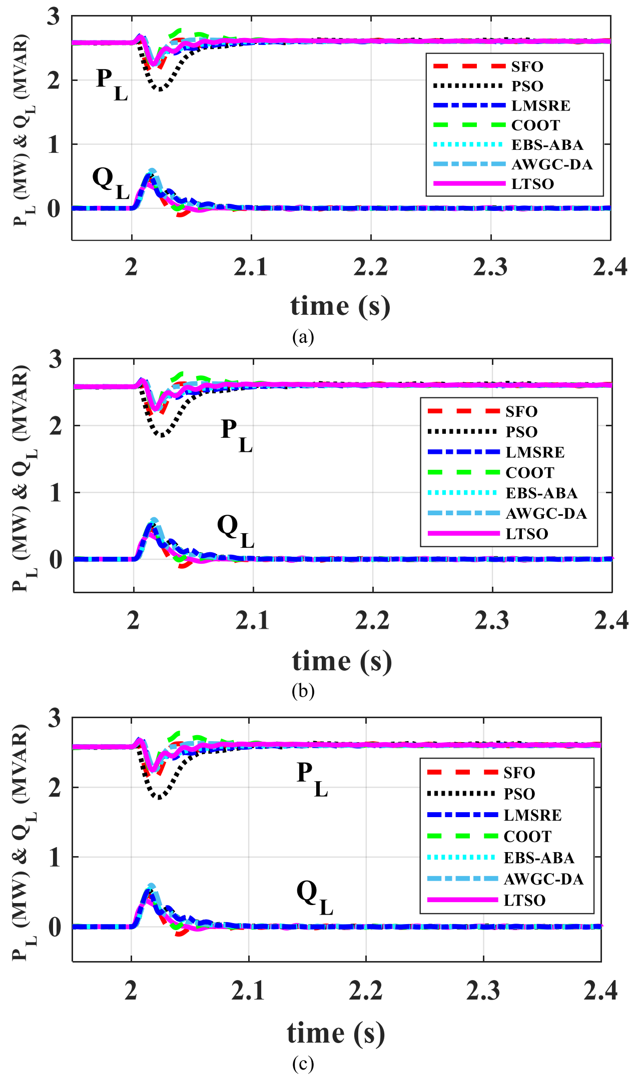

FIGURE 5. The load powers of LTSO, LMSRE, EBS-ABA, AWGC-DA, SFO, COOT, and PSO for Scenario 1. (a-c) are for DG_1 to DG_3.

The mathematical expression for the levy function $LF(\gamma)$ is presented in (10) [40]:

$$LF(\gamma) = 0.01 \times \frac{u \times \sigma}{|v|^{\frac{1}{\gamma}}},$$

$$\sigma = \left(\frac{\Gamma(1+\gamma) \times \sin\left(\frac{\pi\gamma}{2}\right)}{\Gamma\left(\frac{1+\gamma}{2}\right) \times \gamma \times 2^{\left(\frac{\gamma-1}{2}\right)}} \right)^{\frac{1}{\gamma}} \tag{10}$$

The range of 'v' and 'u' random values between zero and one.

Furthermore, the Weibull distribution function $W_D(u_1)$ may be stated numerically below:

$$W_D(u_1) = e^{\left(\frac{u_1}{v_1}\right)^{\eta}} \tag{11}$$

where 'v_1' and 'η' are the Weibull distribution parameters set to 2 and 1, respectively. The TSO search agent is improved based on one of 4 probabilities, and the new LTSO search agents are estimated as illustrated in (12). The random integer 'r1' value determines how a search agent gets updated.

$$X_{l+1} = \begin{cases} X_l^* + P \times CF \times \left(X_l^* + \left(X_l - D_1 . X_l^* \right) e^{-T} \right) & r_1 < 0.25 \\ \left(X_l^* + \left(X_l - D_1 . X_l^* \right) e^{-T} \right) + P \times rand() \times stepsize2_l & 0.25 \le r_1 < 0.5 \\ \left(X_l^* + e^{-T} \left[\cos(2\pi T) + \sin(2\pi T) \right] \left| X_l - D_1 . X_l^* \right| \right) + P \times rand() \times stepsize3_l & 0.5 \le r_1 < 0.75 \\ X_l^* + P \times CF \times stepsize4_l & r_1 \ge 0.75 \end{cases} \tag{12}$$

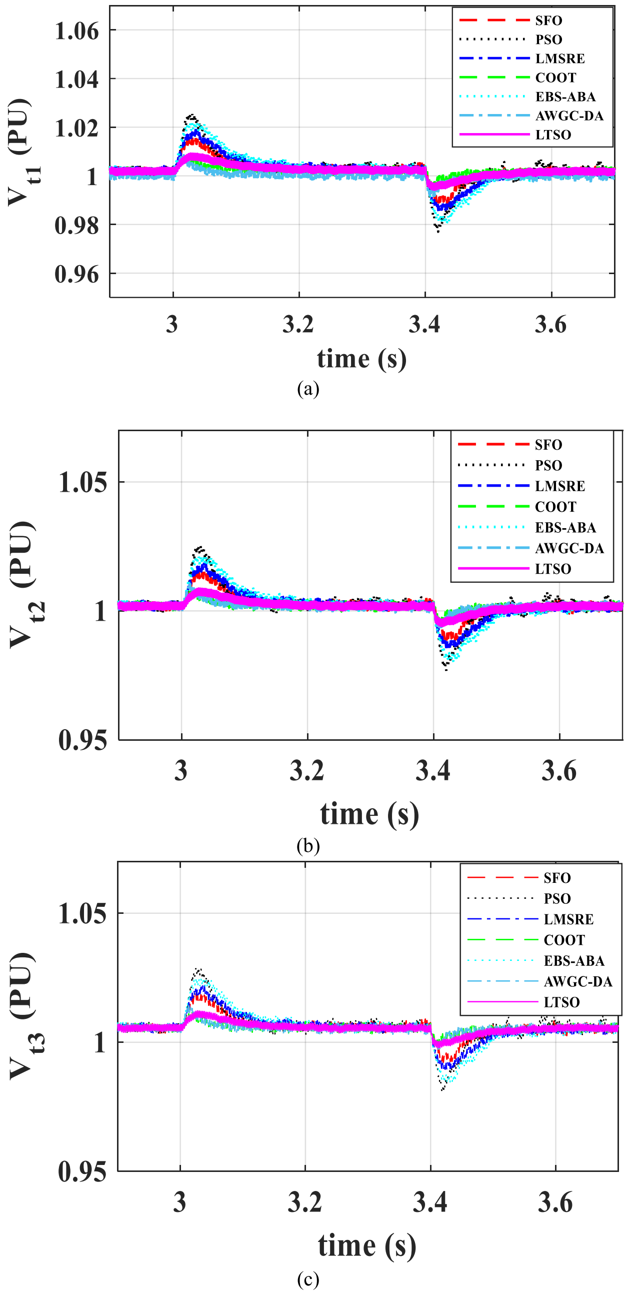

FIGURE 6. The voltages of LTSO, LMSRE, EBS-ABA, AWGC-DA, SFO, COOT, and PSO for Scenario 2. (a-c) are for DG_1 to DG_3.

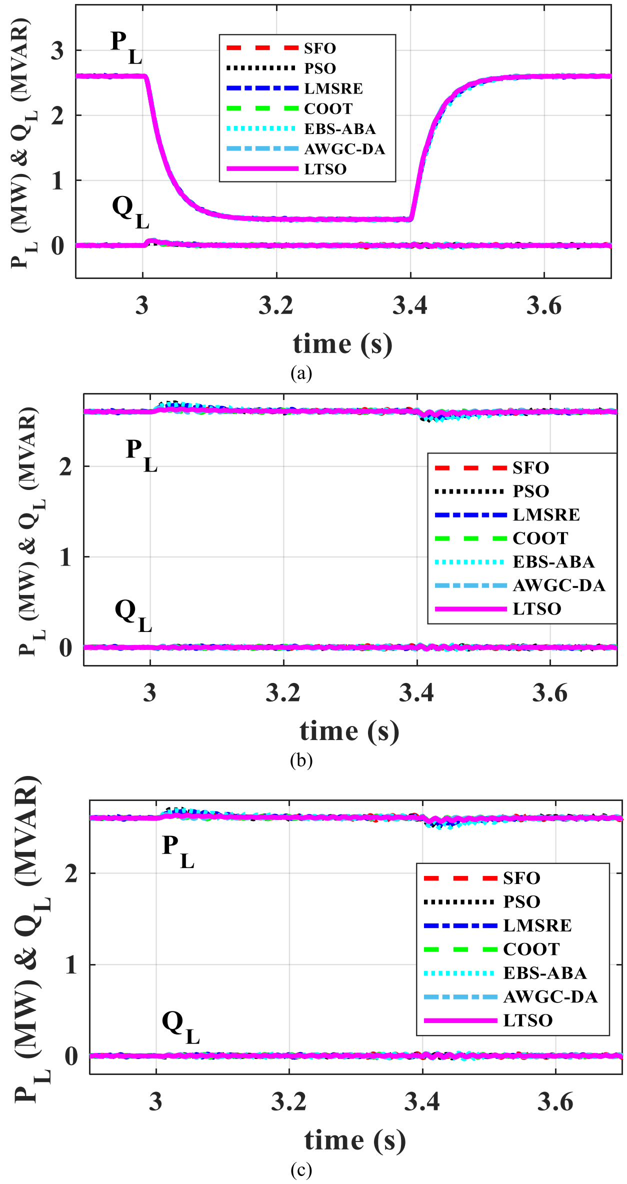

FIGURE 7. The load powers of LTSO, LMSRE, EBS-ABA, AWGC-DA, SFO, COOT, and PSO for Scenario 2. (a-c) are for DG_1 to DG_3.

In this context, the value of 'P' is specified as '0.5', and 'CF' represents a constant that varies with each iteration. Mathematically, the stepsize can be defined as follows:

$$\begin{aligned} stepsize2_l &= W_D *(X_l^* - W_D * X_l) \\ stepsize3_l &= LF * (X_l^* - LF{*}X_l) \\ stepsize4_l &= W_D * W_D *(X_l^* - X_l) \end{aligned} \tag{13}$$

In this context, 'X_l' refers to the current search agent, while X_l^*' represents the best search agent found thus far. The function 'W_D' corresponds to the Weibull distribution function. Additionally, 'LF' stands for a levy function with a constant value, which has been set at 1.5. the overall procedure of LTSO is summarized in the flowchart of Fig. 3.

VI. SIMULATION RESULTS AND DISCUSSION

This section is dedicated to presenting and demonstrating the numerical results obtained during the study, with the primary objective of establishing the validity and effectiveness of the proposed control method based on the LTSO approach. The primary focus of this section is to assess the effectiveness of the proposed control method in maintaining the PCC voltage within specified and desirable ranges. This evaluation is conducted across various operational modes of the MG to determine the controller's ability to ensure stable and reliable voltage levels. The study relies on simulation outcomes obtained from the PSCAD/EMTDC environment. These

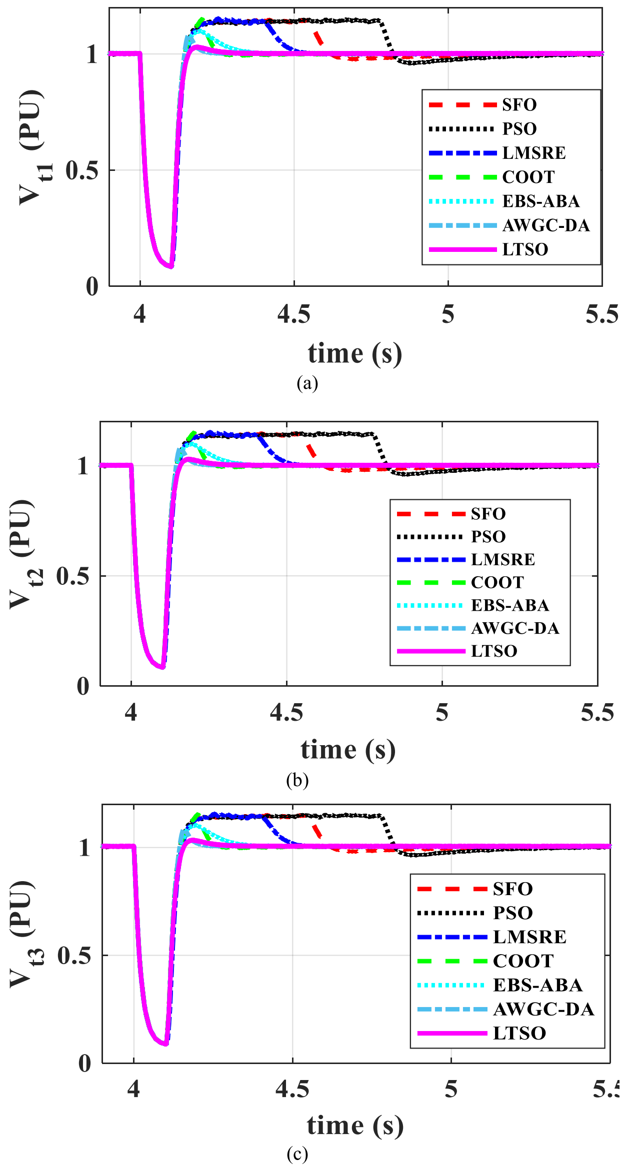

FIGURE 8. The voltages of LTSO, LMSRE, EBS-ABA, AWGC-DA, SFO, COOT, and PSO for Scenario 3. (a-c) are for DG_1 to DG_3.

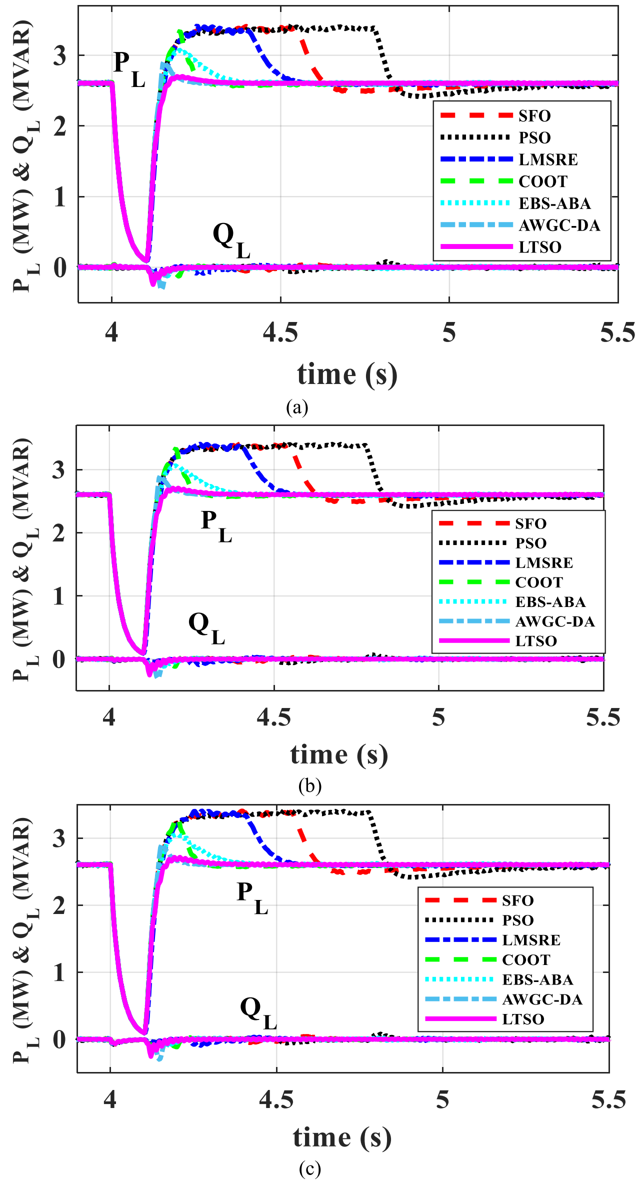

FIGURE 9. The load powers of LTSO, LMSRE, EBS-ABA, AWGC-DA, SFO, COOT, and PSO for Scenario 3. (a-c) are for DG_1 to DG_3.

simulation results are a basis for validating the proposed LTSO and assessing its performance in realistic settings. To establish the superiority and advantages of the LTSO, this section provides a comparative analysis. It compares the results of the LTSO approach to those obtained through alternative control methods, including LMSRE, EBS-ABA, AWGC-DA, SFO, COOT, and PSO techniques [26]. The MG system was tested under different operational scenarios: i) transitioning the system into autonomous mode by disconnecting from the primary grid, ii) adapting to varying load conditions while isolated, and iii) responding to a 3-phase fault while operating in islanded mode.

A. SCENARIO 1 (OFF-GRID MODE)

The initial scenario in this study involves the operation of the MG in a grid-connected status. At the 2-second mark within this scenario, The MG is intentionally disconnected from the grid, shifting into an autonomous status. This transition is a critical test of the MG's self-sufficiency and the effectiveness of the control strategies. During this transition, the study focuses on optimizing the PI parameters of the DGs using various optimization techniques, namely LTSO, LMSRE, EBS-ABA, AWGC-DA, SFO, COOT, and PSO. The resulting PI gains are documented in Table 3, highlighting the fine-tuning required to ensure the MG's stability and performance during the grid disconnection event. Critical parameters are analyzed and compared using various figures to assess the optimized control strategies' performance. Notably, Figure 3a-c presents the voltage profiles of the DGs, comparing the LTSO approach with the other optimization methods (LMSRE, EBS-ABA, AWGC-DA, SFO, COOT, and

TABLE 3. The results of LTSO, LMSRE, EBS-ABA, AWGC-DA, SFO, COOT, and PSO for scenario1.

	LTSO		COOT		SFO		PSO		AWGC-DA	EBS-ABA	LMSRE
Scenario 1 DG 1											
Optimal size	R_1	5.32	R_1	6.212	R_1	6.4212	R_1	2.1473	online	online	online
	R_2	0.00042	R_2	0.0323	R_2	0.0055	R_2	0.00571			
	R_3	2.54	R_3	2.652	R_3	2.953	R_3	1.6794			
	R_4	0.919	R_4	1.912	R_4	0.3473	R_4	0.3393			
MPUT		6.5 %		7.424 %		12.932%		20.41%	7.393%	8.212%	7.931%
T_{stl}		0.0359 s		0.0383 s		0.0344 s		0.0563 s	0.0311 s	0.038 s	0.0451 s
E_{sse}		0.183 %		0.292 %		0.371%		0.422%	0.1931%	0.22%	0.342%
Scenario 1 DG 2											
Optimum size	R_5	5.297	R_5	6.151	R_5	5.983	R_5	1.5693	online	online	online
	R_6	0.000418	R_6	0.0319	R_6	0.0041	R_6	0.00432			
	R_7	2.61	R_7	2.591	R_7	2.5083	R_7	1.2341			
	R_8	0.925	R_8	1.952	R_8	0.2991	R_8	0.30573			
MPUT		6.52 %		7.435 %		12.542%		20.22%	7.372%	8.12%	7.822%
T_{stl}		0.0361 s		0.03826 s		0.0326 s		0.0556 s	0.0308 s	0.0351 s	0.0426 s
E_{sse}		0.1732 %		0.3121 %		0.361%		0.4152%	0.193%	0.193 %	0.321%
Scenario 1 DG 3											
Optimum size	R_9	5.289	R_9	6.041	R_9	5.5344	R_9	1.071	online	online	online
	R_{10}	0.000415	R_{10}	0.0308	R_{10}	0.00315	R_{10}	0.00342			
	R_{11}	2.625	R_{11}	2.512	R_{11}	2.0992	R_{11}	0.996			
	R_{12}	0.9287	R_{12}	1.991	R_{12}	0.2478	R_{12}	0.2591			
MPUT		6.529 %		7.453 %		12.322%		20.052%	7.322%	7.951%	7.642%
T_{stl}		0.03619 s		0.03833 s		0.0318 s		0.0552 s	0.0305 s	0.0341 s	0.0419 s
E_{sse}		0.172 %		0.288 %		0.3541%		0.4083%	0.1891%	0.188%	0.3121%

TABLE 4. The results of LTSO, LMSRE, EBS-ABA, AWGC-DA, SFO, COOT, and PSO for scenario2.

	LTSO		COOT		SFO		PSO		AWGC-DA	EBS-ABA	LMSRE
Scenario 2 DG 1											
Optimal size	R_1	6.13	R_1	6.3742	R_1	6.4681	R_1	1.925	online	online	online
	R_2	0.00051	R_2	0.0011	R_2	0.0125	R_2	0.0119			
	R_3	2.49	R_3	2.541	R_3	2.2796	R_3	2.3124			
	R_4	0.815	R_4	0.9231	R_4	0.2383	R_4	0.2316			
MPUT		0.508 %		0.4912 %		2.206%		3.272%	0.522%	2.3141%	1.912%
MPOT		0.816 %		0.9861 %		2.9672%		3.533%	0.893%	2.9452%	2.2161%
T_{stl}		zero		zero		0.4333 s		0.4533 s	zero	zero	0.4016 s
E_{sse}		0.112 %		0.382 %		0.4534%		0.4961%	0.161%	0.211%	0.4252%
Scenario 2 DG 2											
Optimum size	R_5	6.05	R_5	6.294	R_5	6.0246	R_5	1.4027	online	online	online
	R_6	0.00053	R_6	0.0013	R_6	0.00971	R_6	0.0101			
	R_7	2.487	R_7	2.512	R_7	1.8614	R_7	1.7982			
	R_8	0.813	R_8	0.9181	R_8	0.2077	R_8	0.1998			
MPUT		0.5098 %		0.4922 %		2.152%		3.237%	0.522%	2.241%	1.822%
MPOT		0.82 %		0.964 %		2.9213		3.4571%	0.8916%	2.942%	2.203%
T_{stl}		zero		zero		0.4282 s		0.4473 s	zero	zero	0.4004 s
E_{sse}		0.114 %		0.3923 %		0.4413%		0.492%	0.1621%	0.204%	0.4121%
Scenario 2 DG 3											
Optimum size	R_9	5.096	R_9	6.142	R_9	5.4977	R_9	0.8994	online	online	online
	R_{10}	0.000535	R_{10}	0.00132	R_{10}	0.0067	R_{10}	0.0655			
	R_{11}	2.485	R_{11}	2.4897	R_{11}	1.5786	R_{11}	1.4878			
	R_{12}	0.8112	R_{12}	0.896	R_{12}	0.1753	R_{12}	0.1626			
MPUT		0.511 %		0.4982 %		2.071%		3.212%	0.515%	2.111%	1.814%
MPOT		0.8232 %		0.9472 %		2.908%		3.4363%	0.893%	2.952%	2.1971%
T_{stl}		zero		zero		0.42332 s		0.4182 s	zero	zero	0.3942 s
E_{sse}		0.1167 %		0.413 %		0.435%		0.4861%	0.1622%	0.2011%	0.4031%

TABLE 5. The results of LTSO, LMSRE, EBS-ABA, AWGC-DA, SFO, COOT, and PSO for scenario3.

	LTSO		COOT		SFO		PSO		AWGC-DA	EBS-ABA	LMSRE
					Scenario 3 DG 1						
Optimal size	R_1	6.26	R_1	6.501	R_1	6.1344	R_1	2.1083	online	online	online
	R_2	0.00046	R_2	0.0011	R_2	0.00459	R_2	0.0063			
	R_3	2.53	R_3	2.601	R_3	2.4985	R_3	2.5751			
	R_4	0.93	R_4	0.902	R_4	0.1216	R_4	0.113			
MPUT	91.52 %		92.112 %		91.652%		93.111%		91.541%	92.051%	92.1552%
MPOT	3.02 %		11.551 %		11.692%		11.972%		7.553%	10.52%	12.361%
T_{stl}	0.191 s		0.24472 s		0.5662 s		0.8122 s		0.1892 s	0.221 s	0.49123 s
E_{sse}	0.15 %		0.3113 %		0.471%		0.5491%		0.1951%	0.192%	0.2571%
					Scenario 3 DG 2						
Optimum size	R_5	6.245	R_5	6.3651	R_5	6.232	R_5	2.1791	online	online	online
	R_6	0.000473	R_6	0.00121	R_6	0.00441	R_6	0.0062			
	R_7	2.523	R_7	2.5862	R_7	2.5152	R_7	2.5541			
	R_8	0.934	R_8	0.9463	R_8	0.1194	R_8	0.0993			
MPUT	91.13 %		91.6121 %		91.599%		93.093%		91.16%	91.171%	92.08%
MPOT	3.011 %		11.652 %		11.641%		11.891%		7.42%	10.142%	12.33%
T_{stl}	0.1904 s		0.24461 s		0.5563 s		0.8062 s		0.1882 s	0.2121 s	0.4881 s
E_{sse}	0.1412 %		0.3242 %		0.46871%		0.5463%		0.1931%	0.1843%	0.2522%
					Scenario 3 DG 3						
Optimum size	R_9	6.231	R_9	6.2123	R_9	6.1223	R_9	2.232	online	online	online
	R_{10}	0.000481	R_{10}	0.00136	R_{10}	0.0047	R_{10}	0.0063			
	R_{11}	2.517	R_{11}	2.5231	R_{11}	2.4754	R_{11}	2.5132			
	R_{12}	0.937	R_{12}	0.9672	R_{12}	0.1212	R_{12}	0.01088			
MPUT	91.11 %		91.262 %		91.435%		92.89%		91.142%	91.174%	91.861%
MPOT	2.995 %		12.113 %		11.592%		11.82%		7.399%	10.142%	12.23%
T_{stl}	0.1897 s		0.2494 s		0.554 s		0.7951 s		0.1875 s	0.213 s	0.484 s
E_{sse}	0.1402 %		0.4342 %		0.468%		0.5425%		0.1912%	0.1841%	0.251%

PSO). Additionally, Figures 5a-c depict the complex power profiles of the DGs utilizing the LTSO method alongside the performance of the alternative optimization techniques. The analysis of these figures and associated metrics reveals that the LTSO approach outperforms the other methods in terms of critical performance indicators. Specifically, the MPUT for the autonomous status achieved by the proposed method is less than 6.6%, revealing robust control and limited voltage deviations (Figure 4a). Moreover, the proposed technique achieves a T_{stl} of 36 milliseconds, satisfying the 2% criteria for rapid response and system stability. The E_{sse} is equal to 0.18%, reflecting precise and reliable control. Overall, the initial scenario involves a controlled transition from grid-connected to autonomous mode, optimizing the PI gains for DGs using various techniques. The results demonstrate that the AWGC-DA approach minimizes overshoots, achieves rapid damping, and ensures precise control compared to alternative optimization strategies, thus highlighting its strength, reliability, and functionality in microgrid control.

B. SCENARIO 2 (LOAD CHANGING)

In the second scenario, the MG continues its operation autonomously. During this scenario, the MG's performance is evaluated in response to a dynamic load profile, introducing variability and fluctuations in the load conditions: at t = 3 seconds, a significant change occurs in the load profile. Specifically, the resistance R_{Ll2} is increased to 300 Ω, and shortly after the load increase, at t = 3.4 seconds, R_{Ll2} is decreased to 150 Ω.

To assess and optimize the performance of the MG under these dynamic load conditions, PI parameters for the DGs are optimized using several techniques, including LTSO, LMSRE, EBS-ABA, AWGC-DA, SFO, COOT, and PSO. The optimized PI gains are presented in Table 4. To evaluate the impact of these optimized gains, various figures are used for comparison:

Figures 6a-c: these figures compare the voltage profiles of the DGs using the LTSO approach with those achieved using the other optimization methods (LMSRE, EBS-ABA, AWGC-DA, SFO, COOT, and PSO).

Figures 6a-c depict the DGs' complex power profiles, again comparing the LTSO approach with alternative optimization techniques.

The analysis of these figures and associated metrics reveals the impressive performance of the proposed LTSO controller in the face of dynamic load variations. Notably, the LTSO approach achieves a T_{stl} of zero seconds, satisfying the 2% criteria for rapid response and system stability. The E_{sse} is

TABLE 6. PSCAD for Scenario 1.

Exp.	KP_1	TI_1	KP_2	TI_2	B_1	B_3	B_4	B_5	B_7	B_8	B_9	B_{11}	B_{12}
1	0	0	0	0	14.872	0.142	0.7527	15.2641	0.1495	0.621	15.828	0.16088	0.6288
2	-1	1	1	1	26.513	0.1831	1.053	26.821	0.1857	0.7331	27.301	0.22121	1.021
3	1	1	1	1	12.232	0.28545	0.694	12.513	0.2994	0.513	12.921	0.34661	0.539
4	-1	-1	-1	-1	18.733	0.10671	0.284	19.111	0.10124	0.372	19.621	0.08741	1.045
5	1	0	0	0	11.574	0.16888	0.801	11.9172	0.17972	0.5401	12.381	0.19974	0.72186
6	-1	-1	1	1	30.222	0.29412	1.241	30.583	0.3273	0.9561	30.961	0.3771	0.388
7	0	0	0	0	14.873	0.142	0.7527	15.2642	0.1495	0.611	15.828	0.16088	0.6288
8	1	-1	-1	-1	11.413	0.07992	0.378	11.722	0.0806	0.362	12.071	0.0851	0.931
9	1	-1	1	1	14.322	0.26341	0.587	14.622	0.2799	0.4171	15.092	0.31032	0.659
10	0	0	0	1	14.943	0.14989	0.779	15.2891	0.152	0.5952	15.804	0.16911	0.449
11	0	0	0	-1	15.382	0.16351	0.484	15.733	0.15256	0.321	16.291	0.16622	0.9877
12	-1	1	1	-1	27.423	0.18272	0.515	27.722	0.18584	0.793	28.231	0.21631	1.541
13	0	0	0	0	14.872	0.142	0.7527	15.2642	0.1495	0.621	15.828	0.16088	0.6288
14	0	0	0	0	14.873	0.143	0.7527	15.2641	0.1495	0.621	15.828	0.16088	0.6288
15	1	1	-1	-1	9.342	0.0801	0.308	9.683	0.083	0.3662	10.101	0.09388	1.121
16	0	0	0	0	14.872	0.142	0.7527	15.2641	0.1495	0.621	15.828	0.16087	0.6288
17	1	1	-1	1	8.993	0.07772	0.566	9.3152	0.0804	0.38681	9.667	0.09077	0.702
18	-1	-1	-1	1	18.972	0.1071	0.665	19.421	0.1065	0.4762	19.811	0.09281	0.623
19	-1	0	0	0	23.621	0.11392	0.7743	23.963	0.1165	0.3181	24.541	0.13011	0.863
20	1	1	1	-1	12.5072	0.28541	0.186	12.793	0.3048	0.7392	13.201	0.35471	1.47
21	-1	1	-1	1	13.372	0.05241	0.601	13.721	0.0529	0.421	14.101	0.05741	0.726
22	0	0	0	0	14.872	0.143	0.7527	15.2641	0.1495	0.611	15.828	0.16086	0.6288
23	0	-1	0	0	13.682	0.13581	0.801	16.763	0.141	0.5852	17.341	0.14931	0.547
24	-1	-1	1	-1	30.312	0.1661	0.241	30.632	0.1964	0.512	31.081	0.24682	1.16
25	1	-1	-1	1	11.063	0.0802	1.691	11.372	0.9809	1.313	11.711	0.0862	0.731
26	1	-1	1	-1	14.252	0.27991	0.435	14.5371	0.291	0.733	14.961	0.34931	1.471
27	0	1	0	0	14.921	0.14671	0.711	15.252	0.15483	0.45761	15.857	0.17142	0.735
28	0	0	0	0	14.872	0.143	0.7527	15.2641	0.1495	0.621	15.828	0.16086	0.6288
29	-1	1	-1	-1	12.583	0.06061	0.205	12.893	0.0582	0.5272	13.251	0.06322	1.256
30	0	0	1	0	17.211	0.2383	0.72	17.5461	0.24678	0.5271	18.031	0.28311	0.57189
31	0	0	-1	0	10.613	0.07171	0.5532	10.913	0.0741	0.3102	11.306	0.08312	0.8388

measured at 0.11%, highlighting the precision and reliability of control. Furthermore, the MPUT for the load variations scenario using the proposed LTSO technique is less than 0.51%. It's important to note that during this scenario, DG_1's power is decreased to 1.3 MW and effectively returned at $t = 3.4$ seconds, while the rest of the DGs respond to these changes.

The results demonstrate the exceptional performance of the LTSO, which minimizes overshoots, achieves rapid damping, and ensures precise control, surpassing the alternative optimization strategies. This underscores the strength, reliability, and functionality of the LTSO approach in managing the MG's response to varying load conditions.

C. SCENARIO 3 (3-PHASE FAULT)

In the third scenario, the MG continues its operation autonomously; then, at $t = 4$ seconds, a controlled 3-phase fault is intentionally applied at PCC1. This fault introduction simulates a short-term electrical fault condition and evaluates the MG's response to such disruptions. The applied 3-phase fault is removed at $t = 4.1$ seconds, allowing the MG to recover from the fault condition. This event demonstrates the MG's resilience and ability to restore normal operations.

To assess and optimize the performance of the MG under these dynamic fault conditions, PI parameters for the DGs are optimized using several techniques, including LTSO, LMSRE, EBS-ABA, AWGC-DA, SFO, COOT, and PSO.

TABLE 7. PSCAD results for scenario 2.

Exp.	KP_1	TI_1	KP_2	TI_2	B_1	B_2	B_3	B_4	B_5	B_6	B_7	B_8	B_9	B_{10}	B_{11}	B_{12}
1	0	0	0	0	2.9621	3.956	0.4793	0.267	3.222	3.517	0.49678	0.569	3.972	2.701	0.5881	1.481
2	-1	1	1	1	5.321	7.761	0.6468	0.423	5.333	7.198	0.65771	0.674	5.793	6.311	0.7327	1.301
3	1	1	1	1	2.373	4.161	0.4881	0.551	2.523	3.789	0.5078	0.8015	3.133	3.021	0.6187	1.491
4	-1	-1	-1	-1	4.342	5.144	0.4741	0.285	4.522	4.684	0.48311	0.417	5.2351	3.801	0.5108	1.471
5	1	0	0	0	2.2732	3.324	0.4631	0.208	2.5191	2.8889	0.48852	0.64	3.2832	2.12	0.593	1.481
6	-1	-1	1	1	5.652	7.671	0.6217	0.325	5.653	7.161	0.63021	0.106	5.993	6.361	0.6748	0.821
7	0	0	0	0	2.9622	3.956	0.4793	0.267	3.223	3.517	0.49678	0.569	3.972	2.701	0.5882	1.481
8	1	-1	-1	-1	3.1221	3.671	0.4741	0.462	3.362	3.191	0.4831	0.391	4.002	2.401	0.5133	1.312
9	1	-1	1	1	2.443	4.851	0.5078	0.179	2.593	4.501	0.51332	0.573	3.133	3.757	0.6075	1.174
10	0	0	0	1	2.811	4.071	0.4691	0.438	3.0101	3.641	0.4825	0.39	3.632	2.931	0.5075	1.111
11	0	0	0	-1	3.7291	4.371	0.5382	1.446	4.083	3.871	0.5608	1.743	5.1332	2.801	1.002	2.932
12	-1	1	1	-1	6.342	7.111	0.7302	0.981	6.523	6.601	0.793	1.491	7.363	5.561	1.121	0.451
13	0	0	0	0	2.9622	3.956	0.4791	0.267	3.222	3.517	0.49678	0.569	3.973	2.701	0.5881	1.481
14	0	0	0	0	2.9622	3.956	0.4793	0.267	3.222	3.517	0.49678	0.569	3.972	2.701	0.5883	1.481
15	1	1	-1	-1	3.152	3.881	0.4828	0.365	3.422	3.451	0.49412	0.635	4.262	2.571	0.5443	1.751
16	0	0	0	0	2.9622	3.956	0.4793	0.267	3.223	3.517	0.49678	0.569	3.972	2.701	0.5883	1.481
17	1	1	-1	1	2.742	3.921	0.4799	0.501	2.863	3.617	0.49372	0.174	3.372	2.917	0.5191	0.964
18	-1	-1	-1	1	4.233	5.291	0.4741	0.569	4.263	4.931	0.47487	0.281	4.673	4.251	0.4858	0.837
19	-1	0	0	0	4.522	6.596	0.5328	0.22	4.721	6.181	0.54382	0.839	5.363	5.325	0.5972	1.681
20	1	1	1	-1	3.873	4.731	0.7302	1.405	4.152	4.311	0.82781	1.913	5.092	3.311	1.312	2.161
21	-1	1	-1	1	3.782	5.251	0.4801	0.484	3.843	4.897	0.493	0.222	4.321	4.161	0.5132	0.981
22	0	0	0	0	2.963	3.956	0.4791	0.267	3.222	3.517	0.49678	0.569	3.972	2.701	0.5881	1.481
23	0	-1	0	0	3.052	4.101	0.4747	0.312	3.2902	3.661	0.493	0.521	4.003	2.896	0.5661	1.451
24	-1	-1	1	-1	6.243	6.851	0.6635	1.111	6.411	6.351	0.69672	1.571	7.111	5.36	1.211	1.751
25	1	-1	-1	1	3.143	4.821	0.4802	0.457	3.353	4.321	0.48832	0.201	3.773	3.621	0.5138	0.776
26	1	-1	1	-1	3.462	4.511	0.7161	1.411	3.723	4.101	0.91891	1.921	4.643	3.171	1.4222	3.561
27	0	1	0	0	2.923	3.841	0.4773	0.266	3.172	3.38	0.49951	0.795	3.982	2.537	0.5663	1.721
28	0	0	0	0	2.962	3.956	0.4793	0.267	3.223	3.517	0.49678	0.569	3.973	2.701	0.5881	1.481
29	-1	1	-1	-1	4.483	5.135	0.4802	0.301	4.711	4.641	0.49141	0.691	5.463	3.701	0.5242	1.771
30	0	0	1	0	3.652	6.091	0.5468	0.6368	3.823	5.721	0.56332	0.954	4.473	4.871	0.7908	1.771
31	0	0	-1	0	3.522	4.488	0.4832	0.542	3.632	4.091	0.49121	0.192	4.162	3.349	0.5188	0.9965

The optimized PI gains are presented in Table 5. To evaluate the impact of these optimized gains, various figures are employed for comparison:

Figures 8a-c: these figures compare the voltage profiles of the DGs using the LTSO approach with those achieved using the other optimization methods (LMSRE, EBS-ABA, AWGC-DA, SFO, COOT, and PSO).

Figures 8a-c depict the DGs' complex power profiles, again comparing the LTSO approach with alternative optimization techniques.

The analysis of these figures and associated metrics reveals the impressive performance of the proposed LTSO controller in the face of dynamic load variations. Notably, the LTSO approach achieves a T_{stl} of 19 milliseconds, satisfying the 2% criteria for rapid response and system stability. The E_{sse} is measured at 0.15%, highlighting the precision and reliability of control. Furthermore, the MPOT for the load variations scenario using the proposed LTSO technique is less than 3.1%. The results demonstrate the exceptional performance of the LTSO, which minimizes overshoots, achieves rapid damping, and ensures precise control, surpassing the alternative optimization strategies. This underscores the strength, reliability, and functionality of the LTSO approach in managing the MG's response to varying load conditions.

VII. CONCLUSION

This research presents an innovative methodology for optimizing CSs within islanded MGs by harnessing the capabilities of the LTSO technique. This study's primary focus involves determining optimal gains for Twelve PICs by applying LTSO within a multi-objective optimization framework.

The efficacy and robustness of this approach are convincingly demonstrated through extensive simulations conducted with the PSCAD/EMTDC program. The simulation results confirm the effectiveness of the proposed controller in regulating voltage profiles while simultaneously managing active and reactive powers. Notably, the outcomes reveal rapid and

TABLE 8. PSCAD results for scenario 3.

Exp.	KP_1	TI_1	KP_2	TI_2	B_1	B_2	B_3	B_4	B_5	B_6	B_7	B_8	B_9	B_{10}	B_{11}	B_{12}
1	0	0	0	0	92.392	6.581	1.8868	0.3366	90.113	6.245	1.6902	0.478	87.807	5.521	1.1678	0.772
2	-1	1	1	1	92.293	7.421	3.002	0.329	90.002	7.121	2.6981	100200	87.632	6.551	2.1177	0.586
3	1	1	1	1	92.312	7.531	2.7871	0.401	90.003	7.201	2.682	0.901	87.663	6.635	2.1871	0.551
4	-1	-1	-1	-1	92.542	7.371	5.1361	1.7669	90.312	7.141	5.0044	1.499	88.050	6.834	5.678	0.988
5	1	0	0	0	92.389	6.739	1.8373	0.4939	90.103	6.391	1.6872	0.352	87.793	5.681	1.162	0.808
6	-1	-1	1	1	92.294	7.281	6.9881	1.988	89.989	6.971	6.1551	0.8	87.655	6.371	5.9996	1.451
7	0	0	0	0	92.392	6.581	1.8868	0.3366	90.112	6.245	1.6902	0.478	87.807	5.521	1.1678	0.772
8	1	-1	-1	-1	92.444	7.891	4.311	0.951	90.182	7.7187	4.1351	1.091	87.883	7.381	4.511	0.9
9	1	-1	1	1	92.302	7.461	5.221	7.631	89.992	7.145	4.7661	6.991	87.643	6.531	4.5241	5.499
10	0	0	0	1	92.344	7.601	2.311	0.278	90.035	7.281	2.2231	0.289	87.713	6.66	2.0171	0.335
11	0	0	0	-1	92.677	3.761	0.5542	0.4208	90.511	3.35	0.5296	0.3343	88.255	2.301	0.4791	0.193
12	-1	1	1	-1	92.582	4.771	0.6901	0.531	90.371	4.401	0.6182	1.201	88.111	3.501	0.5294	923.40
13	0	0	0	0	92.393	6.581	1.8868	0.3366	90.113	6.245	1.6902	0.478	87.807	5.521	1.1678	0.772
14	0	0	0	0	92.393	6.581	1.8868	0.3366	90.113	6.245	1.6902	0.478	87.807	5.521	1.1678	0.772
15	1	1	-1	-1	92.542	7.801	3.2031	0.275	90.322	7.611	3.2037	0.458	88.042	7.191	3.2037	0.356
16	0	0	0	0	92.392	6.581	1.8868	0.3366	90.113	6.245	1.6902	0.478	87.807	5.521	1.1678	0.772
17	1	1	-1	1	92.321	8.171	6.221	4.561	89.995	7.911	6.0791	8.761	87.666	7.491	5.9881	6.761
18	-1	-1	-1	1	92.292	8.071	7.1371	1.871	89.975	7.801	7.0581	1.431	87.644	7.34	7.452	0.994
19	-1	0	0	0	92.382	6.901	2.1091	0.56	90.075	6.571	2.0422	0.507	87.759	5.901	1.3203	0.441
20	1	1	1	-1	92.572	4.601	0.6232	0.511	90.352	4.211	0.5758	0.351	88.086	3.291	0.4876	0.376
21	-1	1	-1	1	92.321	7.881	7.1771	8.034	89.982	7.611	6.8552	7.996	87.643	7.24	6.3618	8.121
22	0	0	0	0	92.392	6.581	1.8868	0.3366	90.113	6.245	1.6902	0.478	87.807	5.521	1.1678	0.772
23	0	-1	0	0	92.413	6.591	2.3371	0.25	90.133	6.251	2.2121	0.372	87.803	5.54	1.6648	0.333
24	-1	-1	1	-1	92.553	4.771	0.8898	0.511	90.333	4.411	0.8148	0.461	88.032	3.501	0.6041	0.681
25	1	-1	-1	1	92.293	8.421	6.672	1.781	89.982	8.131	6.483	0.9886	87.663	7.691	6.7071	2.561
26	1	-1	1	-1	92.582	4.941	0.7428	0.751	90.373	4.541	0.6929	0.871	88.082	3.611	0.5301	1.201
27	0	1	0	0	92.428	6.701	1.5372	0.346	90.150	6.361	1.4622	0.286	87.824	5.651	0.9872	0.472
28	0	0	0	0	92.392	6.581	1.8868	0.3366	90.113	6.245	1.6902	0.478	87.807	5.521	1.1678	0.772
29	-1	1	-1	-1	92.553	7.701	6.873	5.601	90.332	7.54	6.5681	5.101	88.052	7.081	6.1271	6.101
30	0	0	1	0	92.383	7.191	2.3621	4.521	90.075	6.861	2.2141	0.348	87.743	6.181	1.6391	0.526
31	0	0	-1	0	92.346	8.031	5.003	7.441	90.048	7.764	4.911	5.501	87.728	7.279	4.611	3.251

effective dampening of transient responses, with minimal settling time (Tstl) and negligible steady-state error (Esse) observed under a range of operational scenarios: i) transitioning the system into autonomous mode by disconnecting from the primary grid, ii) adapting to varying load conditions while isolated, and iii) responding to a 3-phase fault while operating in islanded mode.

To validate the presented LTSO technique further, comprehensive comparative simulations were executed to assess its performance against other optimization strategies, including LMSRE, EBS-ABA, AWGC-DA, SFO, COOT, and PSO approaches. Precisely, in scenario 1, the LTSO approach scaled down the voltage undershoot (MPUT) by 18%, 20.8%, 12%, 49.7%, 12.4%, and 68% compared to the LMSRE, EBS-ABA, AWGC-DA, SFO, COOT, and PSO approaches, respectively. In scenario 2, it scaled down the steady-state error (E_{sse}) by 73.6%, 47%, 30%, 75%, 70.6%, and 77.4% relative to the LMSRE, EBS-ABA, AWGC-DA, SFO, COOT, and PSO approaches, respectively. In scenario 2, adapting to varying load conditions while isolated, the offered approach accomplished a T_{stl} of zero seconds, indicating a speedy response. Moreover, in scenario 3, the LTSO approach scaled down the voltage overshoot (MPOT) by 75.5%, 71.3%, 60%, 74%, 73.8%, and 74.7% compared to the LMSRE, EBS-ABA, AWGC-DA, SFO, COOT, and PSO approaches, respectively. The results establish the superiority of the LTSO approach in enhancing MG behavior during transient events.

The LTSO technique has exhibited significant promise in microgrid control. Future work should focus on expanding its applicability to a broader range of fields, including more complex grid systems, battery storage approaches, and smart-grid systems. An important direction is investigating how LTSO can be leveraged in these domains to enhance overall performance in all types of faults and green energy integration.

ABBREVIATIONS

AWGC-DA	Adaptive-Width Generalized Correntropy Diffusion Algorithm.
CCL	Centralized Control.
COOT	Coot Bird Metaheuristic Optimizer.

TABLE 9. RSM model constants for Scenario 1.

Cons.	scenario (1)								
	B_1	B_3	B_4	B_5	B_7	B_8	B_9	B_{11}	B_{12}
C_1	14.7842	0.14225	0.74641	-0.0084	0.14112	0.5261	15.8971	0.16101	0.63001
C_2	-5.3341	0.01959	0.00471	-5.35	0.07042	0.0165	-5.3761	0.02456	-0.01442
C_3	-1.3941	-0.00782	-0.08142	-1.558	-0.06011	-0.0438	-1.5562	-0.00836	0.08742
C_4	3.8852	0.08221	0.02442	3.87	0.03981	0.0791	3.8981	0.11021	0.04811
C_5	-0.0721	0.0059	0.26991	-0.066	0.05722	0.0615	-0.0792	0.00591	-0.28481
C_6	2.9062	-0.0013	0.0502	2.522	0.01781	-0.009	2.4851	0.0048	0.16212
C_7	-0.3901	-0.0015	0.0181	0.589	0.01761	0.084	0.6232	0.0002	0.01061
C_8	-0.7752	0.0122	-0.1012	-1.189	0.03012	-0.019	-1.3071	0.023	0.07501
C_9	0.4802	0.014	-0.1062	0.093	0.02202	0.01	0.0722	0.0075	0.08802
C_{10}	0.6492	0.01478	-0.07902	0.666	-0.03752	-0.0587	0.6662	0.01983	-0.07952
C_{11}	-2.3931	0.01957	-0.14501	-2.391	-0.03811	-0.0767	-2.3841	0.01629	0.01312
C_{12}	-0.0581	-0.0077	-0.00421	-0.065	0.04792	0.0049	-0.0571	-0.01049	-0.00641
C_{13}	0.3421	0.00325	0.08112	0.342	0.05571	0.0633	0.3542	-0.00517	0.02711
C_{14}	-0.0381	-0.00665	-0.07062	-0.045	-0.06392	-0.0976	-0.0392	-0.00586	-0.01111
C_{15}	-0.0952	0.00863	-0.00841	-0.097	-0.04801	-0.068	-0.0891	0.00666	-0.09052

CS	Control Strategies.
DCL	Droop-Based Control.
DERs	Distributed Energy Resources.
DG	Distributed Generator.
EBS-ABA	Enhanced Block-Sparse Adaptive Bayesian Algorithm.
E_{sse}	Steady-State Error.
LM	Least Mean.
LTSO	Levy Flight and Transient Search Optimization.
MG	Microgrid.
MPOT	Maximum Percentages Overshoot.
MPUT	Maximum Percentages Undershoot.
MVASM	Multivariable And Servomechanism.
PCC	Point of Common Coupling.
PIC	Proportional-Integral Controller.
PSO	Particle Swarm Optimization.
PWM	Pulse Width Modulation.
RESs	Renewable Energy Sources.
RSM	Response Surface Methodology.
SFO	Sunflower Optimization.
SGs	Synchronous Generators.
SRE	Square Root of Exponential.
TSO	Transient Search Optimization.
T_{stl}	Settling Time.
VSIs	Voltage Source Inverters.

NOMENCLATURE

τ	time constant.
α	The damping coefficient.
ω_0	Resonant frequency.
B_1	Maximum Percentages Overshoot.
B_2	Maximum Percentages Undershoot.
B_3	Settling Time.
B_4	Steady-State Error.
$C_1, C_2, \ldots, C_{15}$	the estimated RSMT constants.
CF	constant that varies with each iteration.
K, and P	constant.
KP	Proportional Gain.
LF	a levy function with a constant value.
N_1 and N_2	constants for the second-order differential equation of second-order circuits.
$R_1, R_3, R_5, R_7, R_9, R_{11}$	The proportional Gains of the PI controllers.
$R_2, R_4, R_6, R_8, R_{10}$, R12	the Integral Time Constants of the PI controllers.
T	factor balances the exploration and extraction phases.
TI	Integral Time Constant.
W	weights.
fd	damped frequency.

TABLE 10. RSM model constants for Scenario 2.

Cons.	scenario (2)											
	B_1	B_2	B_3	B_4	B_5	B_6	B_7	B_8	B_9	B_{10}	B_{11}	B_{12}
C_1	3.00121	4.119	0.478791	0.3464	3.25281	3.684	0.49421	0.6427	4.00512	2.867	0.59691	1.573
C_2	-1.01672	-1.0512	-0.01462	0.0477	-0.96742	-1.0253	-0.0014	0.0542	-0.9207	-0.9958	0.01771	0.2013
C_3	-0.03901	-0.0612	0.007102	0.0102	-0.03392	-0.0555	0.00522	0.0796	0.01242	-0.0839	-0.00261	-0.0302
C_4	0.37992	0.6752	0.075551	0.1708	0.37661	0.6627	0.09631	0.3788	0.41631	0.6094	0.21301	0.2023
C_5	-0.34781	0.1339	-0.03458	-0.2123	-0.41352	0.1596	-0.0548	-0.4074	-0.5822	0.2595	-0.16321	-0.4271
C_6	0.3512	0.651	0.02072	-0.224	0.3211	0.656	0.02601	0.012	0.27821	0.663	-0.01202	-0.098
C_7	-0.0602	-0.338	-0.00131	-0.149	-0.0581	-0.358	0.00511	-0.07	-0.05282	-0.343	-0.03971	-0.093
C_8	0.5402	0.981	0.03762	0.1514	0.4371	1.027	0.03712	-0.155	0.27221	1.051	0.04882	-0.295
C_9	0.2191	-0.088	0.02622	0.504	0.2572	-0.123	0.03151	0.339	0.33821	-0.193	0.14831	0.342
C_{10}	0.03412	-0.0903	-0.00527	0.0269	0.02412	-0.0713	-0.0132	-0.0156	0.02561	-0.0672	-0.00291	-0.004
C_{11}	-0.41841	-0.4123	-0.01326	0.036	-0.41091	-0.3763	-0.0005	0.0995	-0.37312	-0.3696	0.01311	0.271
C_{12}	-0.02842	-0.0473	-0.01916	-0.0664	-0.01592	-0.045	-0.0312	-0.013	-0.01061	-0.0489	-0.03652	-0.179
C_{13}	0.04911	0.0397	0.005061	0.0295	0.05291	0.0201	-0.0001	0.0183	0.05062	0.0184	-0.01272	-0.185
C_{14}	-0.12092	-0.1378	-0.00426	0.0414	-0.12962	-0.1296	0.00231	0.0185	-0.13442	-0.1234	0.01782	0.194
C_{15}	-0.18341	-0.0123	-0.03515	-0.2508	-0.18711	-0.0311	-0.0565	-0.2168	-0.20561	-0.0258	-0.14521	-0.023

TABLE 11. RSM model constants for Scenario 3.

Cons.	scenario (3)											
	B_1	B_2	B_3	B_4	B_5	B_6	B_7	B_8	B_9	B_{10}	B_{11}	B_{12}
C_1	92.4021	6.583	1.777	0.8231	90.1215	6.239	1.632	0.494	87.8123	5.508	1.104	-6.813
C_2	-0.00183	0.0781	-0.468	-0.213	-0.00238	0.074	-0.417	0.089	-0.00195	0.068	-0.383	-51.31
C_3	-0.00173	-0.0111	-0.4052	0.1731	0.013891	-0.0071	-0.3642	0.5991	0.01512	-0.007	-0.537	51.824
C_4	0.0155	-0.8531	-1.577	-0.837	0.02012	-0.9081	-1.6142	-1.15	0.01588	-1.075	-1.778	50.213
C_5	0.01054	0.9031	1.3602	0.8651	-0.17168	0.9042	1.2711	0.947	-0.20271	0.9912	1.1791	-50.42
C_6	-0.0283	0.2371	0.3282	-0.864	-0.0414	0.2472	0.3031	-0.081	-0.0424	0.3001	0.2142	16.323
C_7	0.0156	0.0631	0.2922	-1.093	0.0103	0.073	0.276	-0.181	-0.0039	0.1051	0.2991	16.012
C_8	-0.0503	1.0282	2.0361	4.593	-0.06881	1.0792	1.9961	2.416	-0.08181	1.2392	2.0941	17.523
C_9	-0.12707	-0.9021	-0.2182	-1.042	0.1383	-0.9181	-0.1852	-0.197	0.16571	-1.011	0.2222	15.915
C_{10}	0.00463	-0.0551	-0.1051	-0.858	0.005811	-0.0582	-0.0771	-0.612	0.01007	-0.058	0.015	-58.512
C_{11}	-0.0282	-0.0602	0.2344	0.9781	0.01057	-0.0678	0.2522	0.6991	0.01282	-0.07	0.2322	-57.121
C_{12}	0.00825	0.0201	0.0811	0.5062	0.009312	0.0192	0.1032	0.7941	0.01357	0.0191	0.1072	58.314
C_{13}	0.0063	0.00512	-0.4322	-1.327	-0.00819	-0.0001	-0.3672	-1.485	-0.00482	0.0141	-0.23	56.323
C_{14}	-0.00551	-0.0073	-0.4463	-0.181	-0.00695	-0.0092	-0.4032	0.2802	-0.01383	0.0162	-0.442	-57.61
C_{15}	-0.0502	0.5531	0.463	0.0251	-0.01295	0.5903	0.3782	-0.314	-0.01783	0.685	0.358	-58.119

$LF(\gamma)$	the levy function.
r1	random integer.
t,, r1, r2, r3	randomized numbers.
u and v	random values between zero and one.
v_1 and η	the Weibull distribution parameters.
W_D	the Weibull distribution function.
$\boldsymbol{X}_l$	the population's location.
$\boldsymbol{X}_l^*$	best position.
$\boldsymbol{X}_l$	the current search agent.
$\boldsymbol{X}_l^*$	the best search agent found.
z(t)	the dynamic measurement of the voltage over the capacitance of the circuit or the current in the inductor of the circuit.

APPENDIX

See Tables 6–11.

ACKNOWLEDGMENT

The authors extend their appreciation to the Deputyship for Research and Innovation, "Ministry of Education," in Saudi Arabia, for funding this research (IFKSUOR3-328-2).

REFERENCES

[1] H. M. Sultan, A. S. Menesy, S. Kamel, R. A. Turky, H. M. Hasanien, and A. Al-Durra, "Optimal values of unknown parameters of polymer electrolyte membrane fuel cells using improved chaotic electromagnetic field optimization," *IEEE Trans. Ind. Appl.*, vol. 57, no. 6, pp. 6669–6687, Nov. 2021, doi: 10.1109/TIA.2021.3116549.

[2] M. A. Soliman, H. M. Hasanien, A. Al-Durra, and M. Debouza, "High performance frequency converter controlled variable-speed wind generator using linear-quadratic regulator controller," *IEEE Trans. Ind. Appl.*, vol. 56, no. 5, pp. 5489–5498, Sep. 2020, doi: 10.1109/TIA.2020.2996956.

[3] I. Alsaidan, M. A. M. Shaheen, H. M. Hasanien, M. Alaraj, and A. S. Alnafisah, "Proton exchange membrane fuel cells modeling using chaos game optimization technique," *Sustainability*, vol. 13, no. 14, p. 7911, Jul. 2021, doi: 10.3390/su13147911.

[4] M. A. M. Shaheen, H. M. Hasanien, M. S. El Moursi, and A. A. El-Fergany, "Precise modeling of PEM fuel cell using improved chaotic MayFly optimization algorithm," *Int. J. Energy Res.*, vol. 45, no. 13, pp. 18754–18769, Oct. 2021, doi: 10.1002/er.6987.

[5] M. A. Soliman, H. M. Hasanien, H. Z. Azazi, E. E. El-Kholy, and S. A. Mahmoud, "An adaptive fuzzy logic control strategy for performance enhancement of a grid-connected PMSG-based wind turbine," *IEEE Trans. Ind. Informat.*, vol. 15, no. 6, pp. 3163–3173, Jun. 2019, doi: 10.1109/TII.2018.2875922.

[6] A. M. Hussien, R. A. Turky, H. M. Hasanien, and A. Al-Durra, "LMSRE-based adaptive PI controller for enhancing the performance of an autonomous operation of microgrids," *IEEE Access*, vol. 9, pp. 90577–90586, 2021, doi: 10.1109/ACCESS.2021.3091496.

[7] T. Adefarati, R. C. Bansal, M. Bettayeb, and R. Naidoo, "Optimal energy management of a PV-WTG-BSS-DG microgrid system," *Energy*, vol. 217, Feb. 2021, Art. no. 119358, doi: 10.1016/j.energy.2020.119358.

[8] S. Areekkara, R. Kumar, and R. C. Bansal, "An intelligent multi agent based approach for autonomous energy management in a microgrid," *Electr. Power Compon. Syst.*, vol. 49, nos. 1–2, pp. 18–31, Jan. 2021, doi: 10.1080/15325008.2021.1937390.

[9] D. Kumar, H. D. Mathur, S. Bhanot, and R. C. Bansal, "Forecasting of solar and wind power using LSTM RNN for load frequency control in isolated microgrid," *Int. J. Model. Simul.*, vol. 41, no. 4, pp. 311–323, Jul. 2021, doi: 10.1080/02286203.2020.1767840.

[10] A. M. Taher, H. M. Hasanien, A. R. Ginidi, and A. T. M. Taha, "Hierarchical model predictive control for performance enhancement of autonomous microgrids," *Ain Shams Eng. J.*, vol. 12, no. 2, pp. 1867–1881, Jun. 2021, doi: 10.1016/j.asej.2020.12.007.

[11] A. Kumar and T. Ghose, "A Newton–Raphson-based unified load flow of grid-connected and islanded AC–DC microgrids," *Int. Trans. Electr. Energy Syst.*, vol. 31, no. 11, Nov. 2021, Art. no. e13075, doi: 10.1002/2050-7038.13075.

[12] C. Raj D, D. N. Gaonkar, and J. M. Guerrero, "Improved P-f/Q-V and P-V/Q-f droop controllers for parallel distributed generation inverters in AC microgrid," *Sustain. Cities Soc.*, vol. 41, pp. 421–442, Aug. 2018, doi: 10.1016/j.scs.2018.04.026.

[13] R. An, Z. Liu, J. Liu, and B. Liu, "A comprehensive solution to decentralized coordinative control of distributed generations in islanded microgrid based on dual-frequency-droop," *IEEE Trans. Power Electron.*, vol. 37, no. 3, pp. 3583–3598, Mar. 2022, doi: 10.1109/TPEL.2021.3115522.

[14] Z. Özkan and A. M. Hava, "Inductor saturation compensation in three-phase three-wire voltage-source converters via inverse system dynamics," *IEEE Trans. Ind. Electron.*, vol. 69, no. 5, pp. 4309–4319, May 2022, doi: 10.1109/TIE.2021.3084155.

[15] S. D'Arco, J. A. Suul, and O. B. Fosso, "Automatic tuning of cascaded controllers for power converters using eigenvalue parametric sensitivities," *IEEE Trans. Ind. Appl.*, vol. 51, no. 2, pp. 1743–1753, Mar. 2015, doi: 10.1109/TIA.2014.2354732.

[16] M. Saleh, Y. Esa, and A. Mohamed, "Centralized control for DC microgrid using finite state machine," in *Proc. IEEE Power Energy Soc. Innov. Smart Grid Technol. Conf. (ISGT)*, Apr. 2017, pp. 1–5, doi: 10.1109/ISGT.2017.8086062.

[17] W. S. W. Wang, D. E. Davison, and E. J. Davison, "Controller design for multivariable linear time-invariant unknown systems," *IEEE Trans. Autom. Control*, vol. 58, no. 9, pp. 2292–2306, Sep. 2013, doi: 10.1109/TAC.2013.2258812.

[18] Y. K. Bhateshvar and H. D. Mathur, "Power–frequency balance with superconducting magnetic energy storage using optimized intelligent controller," *Energetika*, vol. 60, no. 3, pp. 149–161, Nov. 2014, doi: 10.6001/energetika.v60i3.2988.

[19] A. M. Hussien et al., "Coot bird algorithms-based tuning PI controller for optimal microgrid autonomous operation," *IEEE Access*, vol. 10, pp. 6442–6458, 2022, doi: 10.1109/ACCESS.2022.3142742.

[20] S. Patel, B. Mohanty, and H. M. Hasanien, "Competition over resources optimized fuzzy TIDF controller for frequency stabilization of hybrid micro-grid system," *Int. Trans. Electr. Energy Syst.*, vol. 30, no. 9, pp. 1–20, Sep. 2020, doi: 10.1002/2050-7038.12513.

[21] M. N. Ambia, H. M. Hasanien, A. Al-Durra, and S. M. Muyeen, "Harmony search algorithm-based controller parameters optimization for a distributed-generation system," *IEEE Trans. Power Del.*, vol. 30, no. 1, pp. 246–255, Feb. 2015, doi: 10.1109/TPWRD.2014.2358940.

[22] M. A. M. Shaheen, Z. Ullah, H. M. Hasanien, M. Tostado-Véliz, H. Ji, M. H. Qais, S. Alghuwainem, and F. Jurado, "Enhanced transient search optimization algorithm-based optimal reactive power dispatch including electric vehicles," *Energy*, vol. 277, Aug. 2023, Art. no. 127711, doi: 10.1016/j.energy.2023.127711.

[23] I. Alsaidan, M. A. M. Shaheen, H. M. Hasanien, M. Alaraj, and A. S. Alnafisah, "A PEMFC model optimization using the enhanced bald eagle algorithm," *Ain Shams Eng. J.*, vol. 13, no. 6, Nov. 2022, Art. no. 101749, doi: 10.1016/j.asej.2022.101749.

[24] J. Hu, W. Cao, F. Jiang, L. Hu, Q. Chen, W. Zheng, and J. Zhou, "Study on multi-objective optimization of power system parameters of battery electric vehicles," *Sustainability*, vol. 15, no. 10, p. 8219, May 2023, doi: 10.3390/su15108219.

[25] H. Abubakr, J. M. Guerrero, J. C. Vasquez, T. H. Mohamed, K. Mahmoud, M. M. F. Darwish, and Y. A. Dahab, "Adaptive LFC incorporating modified virtual rotor to regulate frequency and tie-line power flow in multi-area microgrids," *IEEE Access*, vol. 10, pp. 33248–33268, 2022, doi: 10.1109/ACCESS.2022.3161505.

[26] A. M. Hussien, H. M. Hasanien, M. H. Qais, and S. Alghuwainem, "Adaptive-width generalized correntropy diffusion algorithm for robust control strategy of microgrid autonomous operation," *IEEE Access*, vol. 11, pp. 91312–91323, 2023, doi: 10.1109/ACCESS.2023.3308039.

[27] A. M. Hussien, H. M. Hasanien, and S. F. Mekhamer, "Sunflower optimization algorithm-based optimal PI control for enhancing the performance of an autonomous operation of a microgrid," *Ain Shams Eng. J.*, vol. 12, no. 2, pp. 1883–1893, Jun. 2021, doi: 10.1016/j.asej.2020.10.020.

[28] A. M. Hussien, J. Kim, A. Alkuhayli, M. Alharbi, H. M. Hasanien, M. Tostado-Véliz, R. A. Turky, and F. Jurado, "Adaptive PI control strategy for optimal microgrid autonomous operation," *Sustainability*, vol. 14, no. 22, p. 14928, Nov. 2022, doi: 10.3390/su142214928.

[29] A. M. Hussien, S. F. Mekhamer, and H. M. Hasanien, "Cuttlefish optimization algorithm based optimal PI controller for performance enhancement of an autonomous operation of a DG system," in *Proc. 2nd Int. Conf. Smart Power Internet Energy Syst. (SPIES)*, Sep. 2020, pp. 293–298, doi: 10.1109/SPIES48661.2020.9243093.

[30] A. M. Ebid, M. Y. Abdel-Kader, I. M. Mahdi, and I. Abdel-Rasheed, "Ant colony optimization based algorithm to determine the optimum route for overhead power transmission lines," *Ain Shams Eng. J.*, vol. 15, no. 1, Jan. 2024, Art. no. 102344, doi: 10.1016/j.asej.2023.102344.

[31] M. A. M. Shaheen, Z. Ullah, M. H. Qais, H. M. Hasanien, K. J. Chua, M. Tostado-Véliz, R. A. Turky, F. Jurado, and M. R. Elkadeem, "Solution of probabilistic optimal power flow incorporating renewable energy uncertainty using a novel circle search algorithm," *Energies*, vol. 15, no. 21, p. 8303, Nov. 2022, doi: 10.3390/en15218303.

[32] M. Y. Abdel-Kader, A. M. Ebid, K. C. Onyelowe, I. M. Mahdi, and I. Abdel-Rasheed, "(AI) in infrastructure projects—Gap study," *Infrastructures*, vol. 7, no. 10, p. 137, Oct. 2022, doi: 10.3390/infrastructures7100137.

[33] R. Saleh, "A comparative study of particle swarm optimized control techniques for active suspension system," *Int. Rev. Autom. Control*, vol. 15, no. 4, pp. 213–221, Jul. 2022, doi: 10.15866/ireaco.v15i4.22430.

[34] S. S. Reddy and P. R. Bijwe, "Efficiency improvements in meta-heuristic algorithms to solve the optimal power flow problem," *Int. J. Emerg. Electr. Power Syst.*, vol. 17, no. 6, pp. 631–647, Dec. 2016, doi: 10.1016/J.IJEPES.2016.03.028.

[35] H. M. Hasanien, A. S. Abd-Rabou, and S. M. Sakr, "Design optimization of transverse flux linear motor for weight reduction and performance improvement using response surface methodology and genetic algorithms," *IEEE Trans. Energy Convers.*, vol. 25, no. 3, pp. 598–605, Sep. 2010, doi: 10.1109/TEC.2010.2050591.

[36] I. Y. Kim and O. L. de Weck, "Adaptive weighted sum method for multiobjective optimization: A new method for Pareto front generation," *Struct. Multidisciplinary Optim.*, vol. 31, no. 2, pp. 105–116, Feb. 2006, doi: 10.1007/S00158-005-0557-6/METRICS.

[37] M. H. Qais, H. M. Hasanien, and S. Alghuwainem, "Transient search optimization: A new meta-heuristic optimization algorithm," *Int. J. Speech Technol.*, vol. 50, no. 11, pp. 3926–3941, Nov. 2020, doi: 10.1007/s10489-020-01727-y.

[38] M. H. Qais, H. M. Hasanien, and S. Alghuwainem, "Transient search optimization for electrical parameters estimation of photovoltaic module based on datasheet values," *Energy Convers. Manage.*, vol. 214, Jun. 2020, Art. no. 112904, doi: 10.1016/j.enconman.2020.112904.

[39] H. M. Hasanien, M. A. M. Shaheen, R. A. Turky, M. H. Qais, S. Alghuwainem, S. Kamel, M. Tostado-Véliz, and F. Jurado, "Precise modeling of PEM fuel cell using a novel enhanced transient search optimization algorithm," *Energy*, vol. 247, May 2022, Art. no. 123530, doi: 10.1016/j.energy.2022.123530.

[40] M. H. Qais, H. M. Hasanien, and S. Alghuwainem, "Parameters extraction of three-diode photovoltaic model using computation and Harris hawks optimization," *Energy*, vol. 195, Mar. 2020, Art. no. 117040, doi: 10.1016/j.energy.2020.117040.

AHMED M. HUSSIEN received the B.Sc. degree in electrical engineering from the Faculty of Engineering, Future University in Egypt, Cairo, Egypt, in 2014. He is currently pursuing the M.Sc. degree with the Faculty of Engineering, Ain Shams University, Cairo. He is also a TA with the Faculty of Engineering, Future University in Egypt. His research interests include power systems operation, microgrid, and renewable energy systems.

HANY M. HASANIEN (Senior Member, IEEE) received the B.Sc., M.Sc., and Ph.D. degrees in electrical engineering from the Faculty of Engineering, Ain Shams University, Cairo, Egypt, in 1999, 2004, and 2007, respectively. From 2008 to 2011, he was a Joint Researcher with the Kitami Institute of Technology, Kitami, Japan. From 2011 to 2015, he was an Associate Professor with the College of Engineering, King Saud University, Riyadh, Saudi Arabia. Currently, he is a Professor with the Electrical Power and Machines Department, Faculty of Engineering, Ain Shams University. His research interests include modern control techniques, power systems dynamics and control, energy storage systems, renewable energy systems, and smart grids. He is an Editorial Board Member of *Electric Power Components and Systems* journal. He is a Subject Editor of *IET Renewable Power Generation*, *Frontiers in Energy Research*, and *Electronics* (MDPI). He has authored, coauthored, and edited three books in the field of electric machines and renewable energy. He has published more than 250 papers in international journals and conferences. His biography has been included in Marquis Who's Who in the World for its 28 edition, in 2011. He received the Encouraging Egypt Award for Engineering Sciences, in 2012. He also received the Institutions Egypt Award for Invention and Innovation of Renewable Energy Systems Development, in 2014. He also received the Superiority Egypt Award for Engineering Sciences, in 2019. He has received the Ain Shams University Appreciation Award in Engineering Sciences, in 2022. He was the IEEE PES Egypt Chapter Chair (2020–2022). He is the Editor-in-Chief of *Ain Shams Engineering Journal* (Elsevier).

MOHAMMED H. QAIS (Member, IEEE) received the B.Sc. degree in electrical engineering from Sana'a University, Yemen, in 2007, and the M.Sc. and Ph.D. degrees in electrical engineering from King Saud University, Saudi Arabia, in 2014 and 2020, respectively. Since August 2021, he has been a Postdoctoral Fellow with the Centre for Advances in Reliability and Safety Ltd. (CAiRS), Hong Kong, China. From June 2020 to June 2021, he was a Postdoctoral Researcher with the Electrical Engineering Department, King Saud University. From 2008 to 2011, he was an Electrical Engineer with Yemen Mobile Company, Yemen. Since 2011, he has been a Lecturer (on leave) with the Electrical Engineering Department, Sana'a University. His research interests include AI-based control of grid-connected renewable energy power plants, microgrids, energy management, power system operation and control, and power system protection.

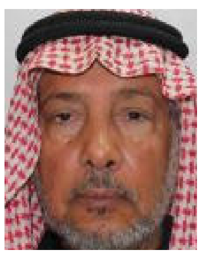

SAAD ALGHUWAINEM (Senior Member, IEEE) received the B.Sc. degree in electrical engineering from King Saud University, Riyadh, Saudi Arabia, in 1974, the M.Sc. degree in electrical engineering from the University of Colorado, Boulder, in 1978, and the Ph.D. degree in electrical engineering from the University of Michigan, Ann Arbor, in 1986. Since 1986, he has been with the Department of Electrical Engineering, King Saud University, where he is currently a Professor. His research interests include renewable energy, power systems operation, control and optimization, power system protection, and electromagnetic transients.